Heinrich Heine
Universität
Düsseldorf

The small ARF-like 2 GTPase TITAN5 is linked with the dynamic regulation of IRON-REGULATED TRANSPORTER 1

Inga Mohr, Monique Eutebach, Marie C. Knopf, Naima Schommen, Regina Gratz, Kalina Angrand, Lara Genders, Tzvetina Brumbarova, Petra Bauer, Rumen Ivanov

Article - Version of Record

Suggested Citation:
Mohr, I., Eutebach, M., Knopf, M. C., Schommen, N., Gratz, R. M., Angrand, K., Genders, L., Brumbarova, T. K., Bauer, P., & Ivanov, R. (2024). The small ARF-like 2 GTPase TITAN5 is linked with the dynamic regulation of IRON-REGULATED TRANSPORTER 1. Journal of Cell Science, 137(23), Article jcs263645. https://doi.org/10.1242/jcs.263645

Wissen, wo das Wissen ist.

UNIVERSITÄTS- UND LANDESBIBLIOTHEK DÜSSELDORF

This version is available at:

URN: https://nbn-resolving.org/urn:nbn:de:hbz:061-20260127-100057-8

Terms of Use:

This work is licensed under the Creative Commons Attribution 4.0 International License.

For more information see: https://creativecommons.org/licenses/by/4.0

© 2024. Published by The Company of Biologists Ltd | Journal of Cell Science (2024) 137, jcs263645. doi:10.1242/jcs.263645

RESEARCH ARTICLE

The small ARF-like 2 GTPase TITAN5 is linked with the dynamic regulation of IRON-REGULATED TRANSPORTER 1

Inga Mohr[1], Monique Eutebach[1], Marie C. Knopf[1], Naima Schommen[1], Regina Gratz[1], Kalina Angrand[1,*], Lara Genders[1], Tzvetina Brumbarova[1], Petra Bauer[1,2,‡] and Rumen Ivanov[1,‡]

ABSTRACT

Iron acquisition is crucial for plants. The abundance of IRON-REGULATED TRANSPORTER 1 (IRT1) is controlled through endomembrane trafficking, a process that requires small ARF-like GTPases. Only few components that are involved in the vesicular trafficking of specific cargo are known. Here, we report that the ARF-like GTPase TITAN5 (TTN5) interacts with the large cytoplasmic variable region and protein-regulatory platform of IRT1. Heterozygous *ttn5-1* plants can display reduced root iron reductase activity. This activity is needed for iron uptake via IRT1. Fluorescent fusion proteins of TTN5 and IRT1 colocalize at locations where IRT1 sorting and cycling between the plasma membrane and the vacuole are coordinated. TTN5 can also interact with peripheral membrane proteins that are components of the IRT1 regulation machinery, like the trafficking factor SNX1, the C2 domain protein EHB1 and the SEC14-GOLD protein PATL2. Hence, the link between iron acquisition and vesicular trafficking involving a small GTPase of the ARF family opens up the possibility to study the involvement of TTN5 in nutritional cell biology and the endomembrane system.

KEY WORDS: ARF-like GTPase, TTN5, IRT1, ARLC1, ARL2, EHB1, Endomembrane system, HALLIMASCH, Iron, PATL2, Plasma membrane, SEC14, SNX1

INTRODUCTION

Plants adjust to environmental changes, such as variations of soil nutrient availability. Cellular membranes are very dynamic in plants, and this is crucial for sessile organisms. Plants can scan their environment for nutrients and control the activities of plasma membrane transporter proteins by vesicular trafficking. Many open questions still exist with regard to the environmental responsiveness and the complexity of the plant cell endomembrane system.

One essential element, iron (Fe), is abundant in the soil. However, given that Fe is mostly present in its ferric Fe^{3+} form in soil, it tends to be immobilized into insoluble complexes. Fe^{3+} must therefore be mobilized into a bioavailable form. Plants like *Arabidopsis thaliana* are capable of this. One mechanism consists of reducing Fe^{3+} via plasma membrane FERRIC REDUCTION OXIDASE 2 (FRO2) (Robinson et al., 1999). The reactive ferrous Fe^{2+} is taken up by IRON-REGULATED TRANSPORTER 1 (IRT1) into root epidermis cells (Eide et al., 1996; Vert et al., 2002).

IRT1 is one of the founding members of an evolutionarily conserved divalent metal ion transporter family named the ZINC-REGULATED TRANSPORTER, ZRT, IRT-LIKE PROTEIN (ZIP) family (Eide et al., 1996; Guerinot, 2000). Because divalent metal ions are potentially cytotoxic, the activity of IRT1, like that of other ZIP proteins, is controlled at the level of protein abundance at the plasma membrane (Connolly et al., 2002; Barberon et al., 2011; Shin et al., 2013; Barberon et al., 2014; Hu, 2021). Importantly, IRT1 protein activity is likely controlled through transport from the *trans*-Golgi network/early endosomes (TGN/EE) to the plasma membrane, degradation by the lytic pathway and recycling back to the plasma membrane (Ivanov et al., 2014). However, the molecular machinery for this process is barely known.

The large cytosolic variable region (vr) between transmembrane domains three and four is a characteristic regulatory feature of ZIP proteins (Guerinot, 2000; Gaither and Eide, 2001). In IRT1, this regulatory variable region, IRT1vr, is crucial for the control of IRT1 abundance. IRT1vr has metal ion-binding sites and residues that can be phosphorylated and ubiquitylated, which are processes that precede vesicular trafficking (Grossoehme et al., 2006; Kerkeb et al., 2008; Dubeaux et al., 2018; Cointry and Vert, 2019). In a search for new components binding with IRT1vr, we identified peripheral membrane proteins that directly or indirectly control the activity of IRT1 (Khan et al., 2019; Hornbergs et al., 2023). Among them is C2-domain protein ENHANCED BENDING 1 (EHB1, also known as CAR6) (Khan et al., 2019), which belongs to the ten-member Ca^{2+}-dependent C2-DOMAIN ABSCISIC ACID-RELATED (CAR) protein family (Rodriguez et al., 2014). CAR proteins act as tethers between the membrane and signaling or transport proteins that are involved in drought, defense or nutrition (Cui et al., 2023). They can also oligomerize and cause membrane deformations, making them candidate proteins to be involved in vesicle budding (Chen et al., 2023). EHB1 interacts with IRT1vr and it has an inhibitory effect on Fe acquisition (Khan et al., 2019). Another IRT1vr interactor is PATELLIN 2 (PATL2). It has a SEC14 domain coupled with a GOLD domain. The SEC14 domain forms a lipid-binding pocket that serves to present or transfer lipophilic substances at membranes (Montag et al., 2023). For example, PATL2 can bind α-tocopherol and it has been proposed that it prevents oxidative stress upon Fe acquisition, possibly by transferring and exchanging phospholipids and α-tocopherol at the membrane (Hornbergs et al., 2023). PATL2 might also initiate vesicle formation, as it binds proteins of the endomembrane system (Hornbergs et al., 2023).

[1]Institute of Botany, Heinrich Heine University, Universitätsstr. 1, 40225 Düsseldorf, Germany. [2]Cluster of Excellence on Plant Sciences (CEPLAS), Heinrich Heine University, 40225 Düsseldorf, Germany.
*Present address: Department of Biosciences-Plant Biology, Saarland University, 66123 Saarbrücken, Germany.

‡Authors for correspondence (petra.bauer@hhu.de; rumen.ivanov@hhu.de)

I.M., 0000-0003-3496-5516; M.E., 0000-0003-1330-5121; R.G., 0000-0002-8820-7211; T.B., 0000-0002-3104-6795; P.B., 0000-0002-0404-4532; R.I., 0000-0001-7909-4123

This is an Open Access article distributed under the terms of the Creative Commons Attribution License (http://creativecommons.org/licenses/by/4.0), which permits unrestricted use, distribution and reproduction in any medium provided that the original work is properly attributed.

Handling Editor: Michael Way
Received 28 October 2024; Accepted 29 October 2024

Journal of Cell Science (2024) 137, jcs263645. doi:10.1242/jcs.263645

Another hint for the involvement of endomembrane trafficking in IRT1 protein control stems from the observation that SORTING NEXIN 1 (SNX1), a crucial component of the retromer complex for transmembrane protein sorting, binds to endomembrane structures containing IRT1, and it is a positive regulator of IRT1 recycling at the TGN (Ivanov et al., 2014). However, IRT1 does not seem to bind SNX1 directly.

Altogether, it looks like IRT1vr has a regulatory role as protein interaction platform to recruit components for vesicular trafficking of IRT1. Fe acquisition is affected by regulation of the vesicular transport mechanism, but how this is achieved and which proteins are involved are open questions that still remain largely elusive. Whether and how the various IRT1vr-interacting peripheral membrane proteins might be connected with each other to control localization of a plasma membrane protein like IRT1, is not clear yet.

Cycling of plasma membrane proteins is an important function of endomembrane trafficking (Valencia et al., 2016; Ivanov and Vert, 2021). One protein family involved in this process in mammalian cells and yeast is the Ras superfamily of small GTPases. Small GTPases are important in vesicle-related processes as they function as molecular switches, due to their GTPase activities, to transmit signals. Small GTPases have usually low intrinsic nucleotide exchange and hydrolysis activity, and therefore, require the support of guanine nucleotide exchange factors (GEFs) and GTPase-activating proteins (GAPs). GEFs recruit the inactive, GDP-bound, GTPase to their site of action and lead to nucleotide exchange by GDP release. GTP binding leads to a conformational change of two regions referred to as switch I and II. The active, GTP-loaded, GTPases then exert their function, for example, the recruiting and subsequent assembly of coat proteins by ARF1 or SAR1, until hydrolysis of the GTP by GAPs. Most of the known interactions occur in the active conformation of the GTPases (Sztul et al., 2019; Nielsen, 2020; Adarska et al., 2021). Although the ARF GTPase family is well-studied in mammals, there are only a few well-established examples of an ARF GTPase functioning in plasma membrane protein trafficking in plants, like that of ARF1-GNOM-mediated recycling of auxin carrier PIN FORMED 1 (PIN1), with GNOM being an ARF GEF (Steinmann et al., 1999; Geldner et al., 2003). The presence of 21 ARF and ARF-like (ARL) GTPases encoded by the *Arabidopsis* genome raises the question whether other ARF members might act in endomembrane trafficking and what are their functions in the diverse physiological and nutrient assimilation pathways besides auxin signaling and cell division.

TITAN5 (TTN5), also known as HALLIMASCH (HAL), ARL2 and ARLC1, is an ARF-like protein. It was identified in two independent screens for abnormal embryo mutants arrested soon after egg cell division, indicating a central cellular function (Mayer et al., 1999; McElver et al., 2000), in agreement with its ubiquitous expression in plants (Mohr et al., 2024). TTN5 is more closely related in sequence to human ADP-ribosylation factor-like 2 (HsARL2) than any *Arabidopsis* protein. HsARL2 is associated with very diverse roles in cells, ranging from microtubule development, which have also been identified for yeast and *Caenorhabditis* homologs (Bhamidipati et al., 2000; Fleming et al., 2000; Radcliffe et al., 2000; Antoshechkin and Han, 2002; Tzafrir et al., 2002; Mori and Toda, 2013), adenine nucleotide transport in mitochondria (Sharer et al., 2002) and control of phosphodiesterase activity in cilia (Ismail et al., 2011; Fansa and Wittinghofer, 2016). HsARL2 is not only involved in a diverse set of functions and signaling cascades, but it also binds very different protein partners for that. The same can be expected for TTN5. *TTN5* is expressed in the root epidermis (Mohr et al., 2024), like *IRT1* (Vert et al., 2002). TTN5 is present at the plasma membrane and in the endomembrane compartment, and is among the rare plant small GTPases for which GTPase activities are known. TTN5 can be considered atypical as it does not require a GEF to be in its active GTP-bound form and has a slow GTPase activity relying on a GAP (Mohr et al., 2024). Its unusually high intrinsic GDP-GTP exchange activity, which causes TTN5 to be present predominantly in a GTP-binding form, seems a prerequisite for its dynamic cellular localization and association with the dynamic endomembrane system and potential vesicular trafficking (Mohr et al., 2024). The physiological functions of this small GTPase, on the other hand, relevant during the entire plant life cycle, have remained elusive.

A yeast two-hybrid screen had identified EHB1 and PATL2 as IRT1 regulators (Khan et al., 2019; Hornbergs et al., 2023). We report here, that with this same strategy, we retrieved the HsARL2-related, small GTPase TTN5. We validated protein interactions of TTN5 and IRT1vr as well as the IRT1vr interactome and found a physiological Fe reductase phenotype linked with root Fe acquisition. Colocalization analysis indicated that active GTP-bound TTN5 had a greater degree of colocalization with IRT1 in intracellular vesicles than a mutant TTN5 form. Hence, our work indicates that the dynamic small GTPase TTN5 acts in a nutritional environmental context in the vesicular trafficking system that controls the root Fe transporter IRT1.

RESULTS

TTN5 interacts with the variable region of IRT1

To identify new cytoplasmic proteins regulating IRT1 we had developed a strategy to identify candidate interaction partners of IRT1vr (residues 145–192) and used IRT1vr as bait against a cDNA expression library prepared from Fe-deficient *Arabidopsis* roots (Khan et al., 2019; Hornbergs et al., 2023). We report here that 25 of the colonies (representing 25%) obtained in the reported yeast two-hybrid (Y2H) screen carried a fragment of the coding sequence of the gene AT2G18390, encoding the ARL-type small GTPase TTN5. The interaction was confirmed in a targeted Y2H assay (Fig. 1A). Small GTPases can act as molecular switches in cells due to their rapid reactions and interactions with effectors, and TTN5 might not require a GEF for nucleotide exchange as it has high affinity for GTP (illustrated in Fig. 1B) (Mohr et al., 2024). We further verified the protein interaction in plant cells using bimolecular fluorescence complementation (BiFC), which is visible as a reconstitution of YFP in positively transformed cells that expressed the control marker mRFP (Fig. 1C). We used previously characterized mutants of conserved amino acids in the GTP-binding pocket, Thr30-to-Asn (T30N, previously found to be dominant-negative or fast cycling) and Gln70-to-Leu (Q70L, with reduced GTP hydrolysis activity) (Fig. 1B) (Mohr et al., 2024). Both the cYFP–TTN5^{T30N} and cYFP–TTN5^{Q70L} forms interacted with nYFP–IRT1vr (Fig. 1D,E). The BiFC interactions were specific as neither protein partner was able to bind negative controls in this assay (Fig. 1F,G). We further elucidated whether IRT1vr might discriminate between the conserved TTN5 variant forms using a quantitative analysis of the interaction by Förster resonance energy transfer-acceptor photobleaching (FRET-APB). This approach is based on close-proximity-dependent energy transfer of an excited GFP-tagged TTN5 donor to a mCherry acceptor, here IRT1vr–mCherry. Energy transfer was quantified as FRET efficiency (Fig. 1H–J). FRET efficiencies between all GFP–TTN5 forms and IRT1vr–mCherry were significantly higher compared to the donor-only sample, confirming protein interactions between all TTN5 forms and IRT1vr. As final evidence, we performed an *in vivo* pulldown experiment to show interaction of full-length IRT1 and

Journal of Cell Science (2024) 137, jcs263645. doi:10.1242/jcs.263645

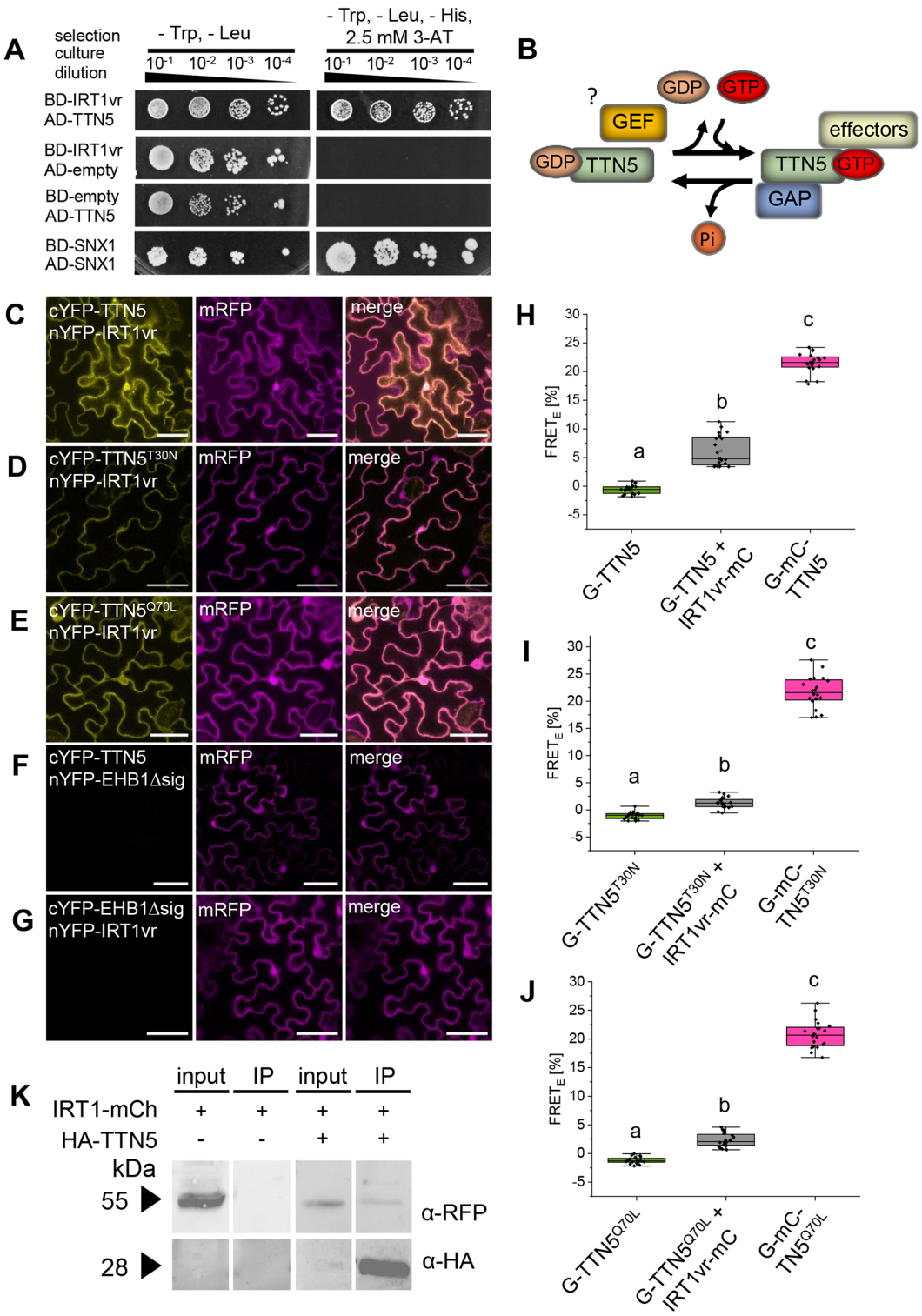

Fig. 1. See next page for legend.

TTN5 (Fig. 1K) using an *Arabidopsis* plant line expressing IRT1–mCherry together with hemagglutinin-tagged (HA)–TTN5. The mCherry part was integrated in the first small cytosolic loop of IRT1 at position 80 (proIRT1::IRT1Q80–mCherry, hereafter IRT1–mCherry), and we determined that this fusion protein was functional as it fully complemented the severe *irt1-1* (SALK_054554) Fe deficiency phenotype (Fukao et al., 2011) (Fig. S1). pro35S::HA_3-TTN5 (hereafter HA_3–TTN5) was also functional as it complemented the *ttn5-1* phenotype as previously described (Mohr et al., 2024). We pulled down protein complexes from whole seedlings using anti-HA beads. This resulted in an increased protein abundance of HA_3–TTN5 (28 kDa) in the elution fraction, as expected (Fig. 1K). Importantly, IRT1–mCherry was simultaneously co-precipitated and detected in this elution fraction whereas it was not detected in a control pulldown experiment without HA_3–TTN5 (Fig. 1K), indicating that the two full-length proteins interact closely in *Arabidopsis* plant cells.

Journal of Cell Science

Journal of Cell Science (2024) 137, jcs263645. doi:10.1242/jcs.263645

Fig. 1. TTN5 interacts with IRT1 via the cytosolic loop and variable region IRT1vr. (A) Targeted Y2H assay between BD-IRT1vr (the IRT1 variable region, vr) and AD-TTN5. Yeast co-transformation samples were spotted in 10-fold dilution series (OD_{600}=10^1–10^4) on double selective (LW; control) and triple selective +0.5 mM 3-AT (LWH, selection for protein interactions) SD-plates. BD-SNX1/AD-SNX1, positive control (Pourcher et al., 2010); BD-IRT1vr/AD-empty and BD-empty/AD-TTN5 are respective negative controls. Experiment was performed three times. (B) Schematic representation of the switching mechanism of small GTPases based on TTN5. TTN5 can switch between an inactive GDP-loaded form to an active GTP-loaded one. Many small GTPases require a GEF for nucleotide exchange (Vernoud et al., 2003). However, TTN5 has unusually high intrinsic GDP to GTP nucleotide exchange capability and help by a GEF might not be needed (indicated by the space between TTN5 and GEF). Nevertheless, it is not excluded that TTN5 can interact with a GEF (indicated by a question mark) in plant cells. GTP hydrolysis has to be catalyzed by a GTPase-activating protein (GAP) (Mohr et al., 2024). GTP-loaded TTN5 can interact with effector proteins for signal transition. (C–G) Validation of TTN5–IRT1vr interaction by BiFC of split YFP. Proteins of interest are fused either to the C- or N-terminal half of split-YFP in this assay. Potential interaction is indicated by a reconstituted YFP signal. mRFP serves as a transformation control. (C–E), nYFP–IRT1vr showed YFP complementation in combination with (C) cYFP–TTN5, (D) cYFP–$TTN5^{T30N}$ and cYFP–$TTN5^{Q70L}$ variants. The complementation predominantly takes place in nucleus and cytoplasm. (F,G) The combinations of (F) cYFP–TTN5 and nYFP–EHB1Δsig, and (G) cYFP–EHB1Δsig and nYFP–IRT1vr served as negative controls. Each combination was tested a minimum of three times with comparable results. Scale bars: 50 µm. (H–J) Confirmed interaction via FRET-APB. A significant increase of FRET efficiency ($FRET_E$) between IRT1vr–mCherry (IRT1vr-mC) and (H) GFP–TTN5 (G-TTN5), (I) GFP–$TTN5^{T30N}$ (G-$TTN5^{T30N}$) or (J) GFP–$TTN5^{Q70L}$ (G-$TTN5^{Q70L}$) indicate short protein distances between the molecules. GFP fusions are donor-only samples and serve as a negative control. GFP–mCherry-tagged constructs show intra-molecular FRET as a respective positive control. Each combination was tested a minimum of three times with comparable results with 20 individual measurements (n=20). The box represents the 25–75th percentiles, and the median is indicated. The whiskers show the 5–95th percentiles. One-way ANOVA with Tukey post-hoc test was performed. Different letters indicate statistical significance between the groups (P<0.05). (K) *In vivo* co-IP experiment demonstrating interaction between full-length IRT1–mCherry (proIRT1::IRT1Q80-mCherry) and HA_3–TTN5 (pro35S::HA_3-TTN5) using *Arabidopsis* roots carrying both transgenes or only IRT1–mCherry grown in parallel under Fe-deficient conditions. Following protein complex extraction, co-IP was conducted with anti-HA antibody. HA_3–TTN5 protein was enriched by the pull down, resulting in an increased band intensity in the elution (IP) fraction compared to the input. IRT1Q80–mCherry protein was copurified with HA_3-TTN5 in two out of three repetitions. No coimmunoprecipitation is detected in the negative control in the absence of HA_3–TTN5 protein. Input, 1.25%. Blot shown is representative of two successful repeats.

In summary, we conclude that TTN5 interacts with IRT1 through the IRT1vr domain surface. We hypothesize that TTN5 is a potential link in the coordination of IRT1 regulation with vesicle trafficking typical for ARF GTPases.

TTN5 affects Fe homeostasis

Following up on the IRT1–TTN5 interaction, we tested whether TTN5 might affect plant growth under Fe-deficient conditions and/or the regulation of the Fe deficiency response. Homozygous *ttn5* knockouts are embryonic lethal (Mayer et al., 1999; McElver et al., 2000), and initial growth experiments with heterozygous plants (*ttn5-1*$^{+/-}$) showed no obvious developmental defects in comparison with wild-type sibling plants under regular growth conditions (Fig. 2A, Fig. S2; Mohr et al., 2024). Likewise, when plants were germinated in Fe-sufficient and -deficient conditions, we did not note any difference in root length. Both, wild-type and *ttn5-1*$^{+/-}$ siblings had increased root length under Fe-deficient conditions (Fig. 2B), as expected in our growth system (Gratz et al., 2019), and there was no difference between them. SPAD values indicating chlorophyll contents were also similar in the wild-type and *ttn5-1*$^{+/-}$ seedlings, indicating that the *ttn5* mutation has no effect on leaf color (Fig. 2C). Also at advanced growth stages, *ttn5-1*$^{+/-}$ plants did not differ in growth and leaf color from their wild-type siblings, neither in in control soil (pH 6.2) nor in an alkaline, calcareous soil (ACS, pH 8). The latter conditions require Fe mobilization capacities given that Fe acquisition is inhibited at high pH values in the presence of bicarbonates, resulting in smaller plants with leaf chlorosis (Ohwaki and Sugahara, 1997; Schmid et al., 2014; Fig. S2B). Both wild-type and *ttn5-1*$^{+/-}$ plants showed similarly lower aerial biomass increase and lower chlorophyll in ACS conditions over a period of 43 days compared to what as seen in the control conditions (Fig. S2A–D). We examined the heterozygous seedlings at the molecular and physiological level. *TTN5* expression was nearly 50% reduced in *ttn5-1*$^{+/-}$ compared to wild-type siblings, consistent with single allele presence (Fig. 2D). Very interestingly, we detected a 15% decrease of *TTN5* gene expression under Fe deficiency compared with Fe sufficiency in both wild-type and *ttn5-1*$^{+/-}$ plants, indicating that TTN5 might be perhaps less needed under low Fe supply (Fig. 2D). *FRO2* encodes an Fe uptake component, the ferric reductase oxidase enzyme (Robinson et al., 1999), that closely interacts with IRT1 in the root plasma membrane (Martín-Barranco et al., 2020). *FRO2* and *IRT1* gene expression increase in response to Fe deficiency, and this serves as a molecular marker for the root Fe deficiency status (e.g. Gratz et al., 2019). No difference of gene expression levels of *FRO2* and *IRT1* occurred in *ttn5-1*$^{+/-}$ roots compared with wild type, and both genes were induced under low Fe versus high Fe as expected (Fig. 2E,F). This indicates that root Fe deficiency responses might not be compromised in *ttn5-1*$^{+/-}$. However, we noted that in two out of three experiments (each including the indicated biological replicates), that root Fe reductase activity was altered; it was up-regulated under Fe-deficient versus -sufficient conditions in wild-type and *ttn5-1*$^{+/-}$ roots, as expected (e.g. Robinson et al., 1999; Gratz et al., 2019) but the induction was lower in *ttn5-1*$^{+/-}$ compared with that in wild-type siblings (Fig. 2G).

Taken together, heterozygous *ttn5-1*$^{+/-}$ seedlings have an Fe reductase phenotype that indicates that TTN5 has a positive effect of at the physiological level on Fe acquisition responses in the plasma membrane. This was interesting, because the two other interactors of IRT1vr, EHB1 and PATL2, have an opposite effect on Fe reductase activity (Khan et al., 2019; Hornbergs et al., 2023).

TTN5 colocalizes with IRT1 in the plasma membrane and in vesicles

To investigate whether TTN5 might be located in similar places to IRT1 in root cells, as expected for interacting proteins, we grew and compared side by side localization of fluorescent signals in *Arabidopsis* plant roots expressing either IRT1–mCitrine (proIRT1::IRT1–mCitrine/*irt1-1*; described in Dubeaux et al., 2018), or YFP–TTN5 (pro35S::YFP–TTN5; described in Mohr et al., 2024). A similar approach has been used to compare intracellular localization of IRT1 and PATL2 fusion proteins in root cells (Hornbergs et al., 2023). As previously described, the fluorescence signal of IRT1–mCitrine was present at the plasma membrane of root epidermis cells in our growth system (Fig. S3A) (Dubeaux et al., 2018; Hornbergs et al., 2023). A fluorescence signal at the plasma membrane was also detected for YFP–TTN5-expressing seedlings (Fig. S3B), and this corresponded to the previously identified pattern (Mohr et al., 2024). Virtual cross sections of both roots highlighted the described polar localization for IRT1–mCitrine, visible in only a

Journal of Cell Science (2024) 137, jcs263645. doi:10.1242/jcs.263645

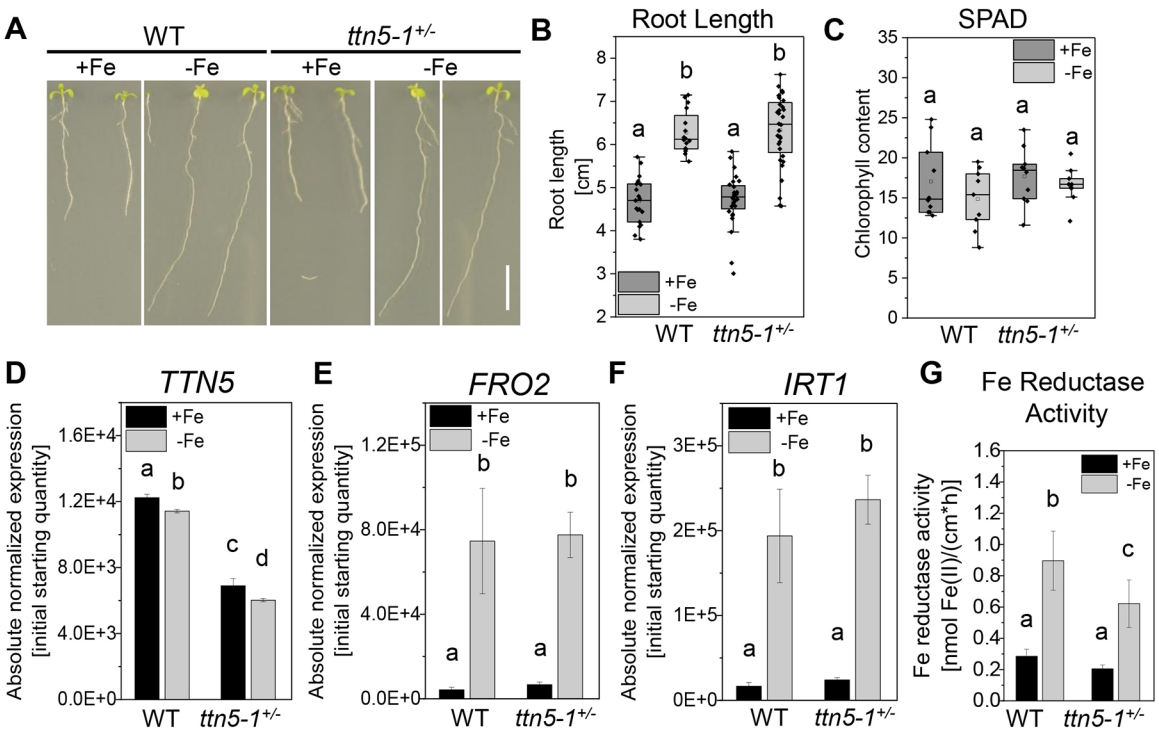

Fig. 2. Heterozygous *ttn5-1*$^{+/-}$ seedlings can have an Fe reductase phenotype. Heterozygous *ttn5-1*$^{+/-}$ and their wild-type (WT) sibling seedlings were grown on Hoagland plates with (+Fe) or without (–Fe) Fe for 10 days (A,B) or in the 2-week system (C–G). All plants were individually genotyped as WT or *ttn5-1*$^{+/-}$. Note that homozygous *ttn5-1*$^{-/-}$ is embryonic lethal. (A) + and –Fe-grown *ttn5-1*$^{+/-}$ seedlings were phenotypically indistinguishable from WT siblings. Scale bar: 1 cm. (B) Quantified root length of results from A. Root length increased under Fe-deficient conditions (–Fe, light gray boxes) compared to in sufficient conditions (+Fe, dark gray boxes) in a similar manner in both *ttn5-1*$^{+/-}$ and WT siblings (+Fe: WT n=19; *ttn5-1*$^{+/-}$ n=28; –Fe: WT n=16; *ttn5-1*$^{+/-}$ n=32). (C) SPAD values, reflecting chlorophyll amounts, were similar under both Fe conditions (–Fe, light gray boxes; +Fe, dark gray boxes) and comparable between the plants (+Fe: n=10; –Fe: n=9). For B and C, the box represents the 25–75th percentiles, and the median is indicated. The whiskers show the 5–95th percentiles. (D–F) Gene expression data determined by RT-qPCR of *TTN5, FRO2* and *IRT1* in *ttn5-1*$^{+/-}$ roots compared to WT siblings in Fe-sufficient (+Fe, black bars) or -deficient (–Fe, gray bars) conditions. (D) *TTN5* expression levels were higher in +Fe than –Fe conditions in WT and *ttn5-1*$^{+/-}$ seedlings. Expression was about half in mutant versus WT. (E,F) *FRO2* and *IRT1* expression was induced upon Fe deficiency versus sufficiency in WT and *ttn5-1*$^{+/-}$ seedlings in comparable amounts. Data was obtained from three biological replicates (n=3). (G) Root ferric reductase activity determined by the Fe^{2+}-ferrozine assay at 562 nm. Iron reductase activity was increased upon Fe deficiency in WT. The same was found in *ttn5-1*$^{+/-}$ sibling seedlings under Fe deficiency but to a lesser extent. The assay was performed with three (WT) and four (*ttn5-1*$^{+/-}$) biological replicates (WT n=3; *ttn5-1*$^{+/-}$ n=4). The experiment was repeated in total three times. In two cases, Fe reductase activity was reduced in *ttn5-1*$^{+/-}$ compared with WT siblings (one representative experiment shown), and once it was not different. One-way ANOVA with Tukey as post-hoc test was performed. Different letters indicate statistical significance between the groups (P<0.05).

very few epidermis cells, as previously seen (Fig. S3C; Dubeaux et al., 2018; Hornbergs et al., 2023) compared with an equally distributed YFP localization in the plasma membrane for YFP–TTN5-expressing seedlings in the epidermis (Fig. S3D). Next to plasma membrane localization, the fluorescence signals of both of IRT1–mCitrine- and YFP-TTN5-expressing seedlings were also present in vesicle-like structures in root cells (Fig. S3E,F). These findings suggest that, indeed, IRT1 and TTN5 locate to similar structures inside root cells, supporting an interaction at these places.

To confirm the obtained *Arabidopsis* data and to investigate potential colocalization of TTN5 with IRT1 in the same cells, we used the transient expression system of *Nicotiana benthamiana*. This system has the advantage that fusion proteins of TTN5 and IRT1 are well detectable, and through well-established pharmacological approaches, the localization patterns of TTN5 and IRT1 proteins can be confirmed (Ivanov et al., 2014; Mohr et al., 2024). We used a GFP-tagged IRT1 with GFP inserted inside IRT1vr (hereafter termed IRT1–GFP). This IRT1 fusion protein was present at the plasma membrane. Fluorescent spots were also found in close proximity to the plasma membrane (Fig. S4A), consistent with previous reports (Barberon et al., 2011; Ivanov et al., 2014). To further evaluate its usefulness for localization studies, we compared IRT1–GFP signals with already described C-terminally tagged IRT1–mCherry signals in *N. benthamiana* pavement cells before and after wortmannin treatment (see Ivanov et al., 2014). Wortmannin is a fungal metabolite with an inhibitory effect on phosphatidylinositol-3-kinase (PI3K) function, leading to swollen multivesicular bodies (MVBs) and is therefore commonly used to investigate endocytosis (Cui et al., 2016). Signals upon expression of these two fusion proteins showed colocalization (Fig. S4B) and, following wortmannin treatment, were observed, as well as at other locations, in swollen structures, suggesting a partial presence in the MVBs (Fig. S4C) and indicating that the IRT1–GFP fusion protein is suitable for IRT1 localization studies. IRT1–GFP also partially complemented an early rosette growth deficit of *irt1-1* (in pro35S::IRT1-GFP/*irt1-1* plants), indicating partial functionality of the IRT1–GFP construct for this trait (Fig. S4D).

We detected colocalization of IRT1–GFP and mCherry–TTN5, including fluorescence signals for mutant TTN5 at the plasma membrane or just below (Fig. 3A–C). Previously, we have described YFP–TTN5 localization in vesicle-like structures and the close proximity of YFP–TTN5 to the plasma membrane (Mohr et al.,

2024). Moving fluorescent structures upon YFP–TTN5^{T30N} expression were less mobile than those seen for YFP–TTN5 and YFP–TTN5^{Q70L} (Mohr et al., 2024). Very interestingly, the different mCherry–TTN5 had different abilities to colocalize with IRT1, as determined by examining Pearson coefficients (Fig. 3D). Whereas the Pearson coefficients of signals of IRT1–GFP with mCherry–TTN5 and mCherry–TTN5^{Q70L} were 0.80 and 0.77, it was higher, namely 0.90, for IRT1–GFP and mCherry–TTN5^{T30N}, demonstrating higher general colocalization between IRT1–GFP and the low-mobile TTN5^{T30N} form (similar results were found with overlap coefficients, Fig. S4E). Signals of all three mCherry–TTN5 forms were also localized in IRT1–GFP-positive structures close to the plasma membrane, suggesting colocalization in plasma membrane-derived vesicles (Fig. 3E–G). Surprisingly, the Pearson coefficients changed when these spotted structures were analyzed (Fig. 3H; Fig. S4F shows similar results for overlap coefficients). Whereas the values for fluorescent signals of mCherry–TTN5 (0.80) and mCherry–TTN5^{Q70L} (0.78) constructs with IRT1–GFP remained relatively similar to those for plasma membrane colocalization, we now obtained, at 0.78, a similar coefficient with mCherry–TTN5^{T30N}. Similar results were achieved upon checking the overlaps of mCherry–TTN5 structures with IRT1–GFP and vice versa with a centroid-based analysis. We obtained overlaps of 36–41% for mCherry–TTN5 signals with IRT1–GFP (Fig. S4G), and 54% for IRT1–GFP-positive structures colocalized with mCherry–TTN5^{T30N} signals, whereas 64% and up to 83% was found for colocalization with mCherry–TTN5 and mCherry–TTN5^{Q70L}, respectively. From this, we hypothesize that IRT1 is more likely to be colocalized with TTN5^{T30N} at the plasma membrane than with wild-type TTN5 or TTN5^{Q70L} as the latter might be active in promoting intracellular cycling. This is consistent with the above observation that mCherry–TTN5^{T30N} signals were slower moving in certain cells than those of the other two TTN5 fusion proteins. We therefore deduce that TTN5^{T30N} might slow down the removal of IRT1 from the plasma membrane. In an attempt to identify the intracellular structures in which colocalization of TTN5 and IRT1 occurred, we treated the cells with wortmannin (Fig. 3I). Structures positive for both IRT1–GFP and mCherry–TTN5 fluorescent signals became doughnut shaped, suggesting that IRT1–TTN5 colocalization occurs in MVBs (Fig. 3J,K). The presence of IRT1 in these late endosomal compartments has been observed previously and might be part of the pathway to IRT1 vacuolar degradation (Dubeaux et al., 2018), as is seen for mCherry–TTN5 (Mohr et al., 2024). Thus, our findings emphasize the involvement of TTN5 in the endomembrane trafficking of the Fe transporter IRT1.

TTN5 interacts with IRT1 regulators EHB1, SNX1 and PATL2

IRT1 can associate and colocalize with peripheral membrane proteins SNX1, EHB1 and PATL2, which are associated with events of vesicular trafficking (Ivanov et al., 2014; Khan et al., 2019; Hornbergs et al., 2023). This opens up the possibility that TTN5 might associate not only with IRT1 but also with proteins of IRT1 interactome in close proximity in cells, prompting us to investigate this further.

At first, we tested the IRT1-interacting protein EHB1. CAR proteins like EHB1 have a plant-specific insertion of an extra region within the C2 domain known as a signature (sig) domain that is involved in binding proteins including IRT1 (Rodriguez et al., 2014; Khan et al., 2019). We demonstrated above that nYFP–EHB1Δsig did not interact with cYFP–TTN5 in BiFC (Fig. 1F). However, when using for interaction with cYFP–TTN5 we did find evidence of protein interaction for the intact nYFP–EHB1 protein and the EHB1 sig-nYFP domain alone being in close proximity to the plasma membrane using BiFC, in contrast to EHB1Δsig (Fig. 4A–C). Surprisingly, the cYFP–TTN5 mutant forms both failed to complement with nYFP–EHB1 in the split-YFP assay (Fig. 4D,E). This was surprising because FRET-APB experiments validated the interaction between EHB1–GFP as the donor and TTN5–mCherry, as well as of the two TTN5 mutant variants, as the acceptors (Fig. 4F). Surprisingly, the FRET pairs EHB1–GFP with TTN5^{T30N}–mCherry and TTN5^{Q70L}–mCherry resulted in an even higher FRET efficiency compared to that seen with TTN5–mCherry (Fig. 4F). It is possible that the mutant behavior and difference between BiFC and FRET-APB were due to the different tag orientations in these two types of assays.

In another BiFC experiment, cYFP–TTN5 was able to complement split-YFP together with SNX1–nYFP close to the plasma membrane (Fig. 4G). The cYFP–TTN5^{T30N} mutant failed in BiFC (Fig. 4H), whereas the hydrolysis impaired TTN5 GTPase variant interacted with SNX1–nYFP (Fig. 4I). SNX proteins are classified by their characteristic domains. SNX1 represents the class I SNX proteins, characterized by the presence of PHOX-homology (PX) and Bin-Amphiphysin-Rvs (BAR) domains (Heucken and Ivanov, 2018). Membrane and phosphoinositide binding is mediated by the PX domain, whereas the BAR domain is involved in membrane curvature sensing and the formation of endosomal tubules (Peter et al., 2004; Frost et al., 2009). Interestingly, ARF GAPs, which are needed for the GTP hydrolysis, contain a BAR domain as well (Memon, 2004). We found evidence that cYFP–TTN5 binds to both the SNX1 PX–nYFP and BAR–nYFP domains using BiFC (Fig. 4J,K).

Finally, it is known that the plasma membrane-localized SEC14 protein PATL2 binds IRT1vr (Hornbergs et al., 2023), hence, we tested interaction ability of cYFP–TTN5 with PATL2–nYFP in BiFC experiments. YFP signals indicating complementation and interaction were visible at the plasma membrane, which is in accordance with the localization studies for both PATL2 and TTN5 (Fig. 4L). We were not able to observe YFP signal complementation for the combination of PATL2–nYFP and either of the two GTPase variants cYFP–TTN5^{T30N} (Fig. 4M) and cYFP–TTN5^{Q70L} (Fig. 4N). This was very interesting as it is either a limitation of the method or could indicate that the TTN5 switching mechanism might be required for a potential interaction between the proteins. However, this needs to be tested further in the future. To further identify the region of interaction, we tested already published deletion mutants of PATL2 (Montag et al., 2020). PATL2 can be divided into two protein halves, consisting of either an N-terminal part with no particular conformation or the C-terminal part with CRAL-TRIO-N-terminal extension (CTN)-SEC14-Golgi dynamics (GOLD) domains, which are conserved among SEC14-GOLD proteins in plants (Montag et al., 2020). The N-terminal part is needed for the interaction with IRT1vr (Montag et al., 2020). We used the PATL2 deletion mutants PATL2ΔC lacking the CTN-SEC14-GOLD part and PATL2ΔN lacking the IRT1vr-interacting N-terminal part. PATL2ΔC–nYFP together with cYFP–TTN5 complemented YFP fluorescence indicating interaction (Fig. 4O), whereas no signal was obtained by PATL2ΔN–nYFP in combination with cYFP–TTN5 (Fig. 4P), which is similar to the case for IRT1vr (Hornbergs et al., 2023). Interestingly, the fluorescent complementation signal between cYFP–TTN5 and PATL2ΔC–nYFP was no longer present at the plasma membrane, consistent with the observation that the PATL2 plasma membrane localization is dependent on the C-terminal PATL2 domain region (Montag et al., 2020).

We also analyzed *EHB1*, *SNX1* and *PATL2* gene expression. All genes were expressed in similar levels in both wild type and

Journal of Cell Science (2024) 137, jcs263645. doi:10.1242/jcs.263645

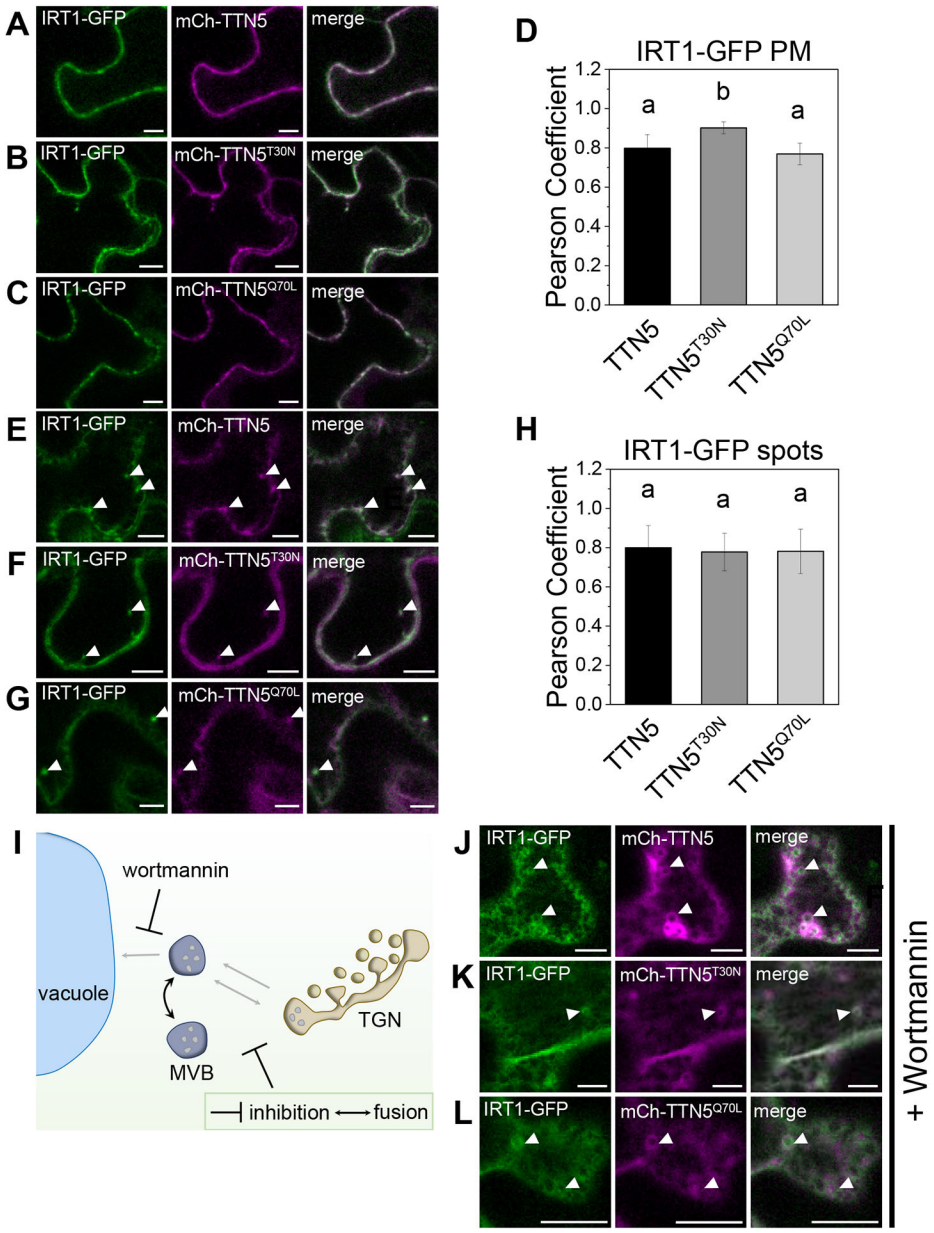

Fig. 3. TTN5 and IRT1 fluorescence protein signals colocalize at the plasma membrane and in MVBs in *N. benthamiana* leaf pavement cells. Fluorescence signals for mCherry–TTN5 and its mutant derivatives mCherry–TTN5^{T30N} and mCherry–TTN5^{Q70L} were colocalized with IRT1–GFP (pro35S::IRT1-GFP) expression in *N. benthamiana* leaf pavement cells. (A–C) Fluorescence signals from mCherry–TTN5 and mCherry–TTN5 variant expression constructs were present at the plasma membrane and in distinct spots together with IRT1–GFP signals. (D) JACoP-based colocalization analysis of mCherry–TTN5 and variants with IRT1–GFP (Bolte and Cordelières, 2006) performed with ImageJ (Schneider et al., 2012). A comparison of Pearson's coefficients for IRT1–GFP with mCherry–TTN5, mCherry–TTN5^{T30N} and mCherry–TTN5^{Q70L} at the plasma membrane (PM). Fluorescence signals from the mCherry–TTN5^{T30N} construct were statistically significant more present at the PM compared to signals of mCherry–TTN5 and mCherry–TTN5^{Q70L}. (E–G) Internalized fluorescence signals of IRT1–GFP expression were present in vesicle-like structures positively labeled by mCherry–TTN5 and mCherry–TTN5 variant signals (arrowheads). (H) Comparison of Pearson's coefficients for IRT1–GFP with mCherry–TTN5, mCherry–TTN5^{T30N} and mCherry–TTN5^{Q70L} in internalized spots. Fluorescence signals for all mCherry–TTN5 constructs colocalized in a similar way with IRT1–GFP signals. (I) Schematic illustration of the inhibiting function of the fungal metabolite wortmannin on cellular trafficking routes between the vacuole and the trans-Golgi network via MVBs, leading to swelling of MVBs. (J–L) Cells were treated with wortmannin (10 µM). Swollen MVBs are visible with the GFP and mCherry channel, respectively. Colocalization is indicated with filled arrowheads. Microscopy experiments were conducted in a minimum of three repetitions ($n \geq 3$). JACoP analyses were performed three times ($n=3$). One-way ANOVA with Fisher-LSD as post-hoc test was performed. Different letters indicate statistical significance between the groups ($P<0.05$). Scale bars: 10 µm.

ttn5-1$^{+/-}$ plants (Fig. S5A–C) indicating that there was no feedback at the level of regulation of genes encoding the TTN5 interactors.

In summary, we show that TTN5 is not only able to interact with IRT1vr but also with three peripheral membrane proteins that can be present in the vicinity of IRT1 at membrane sites in root cells.

DISCUSSION

Here, we report that the small GTPase TTN5 is a potential link in IRT1-related Fe homeostasis and trafficking of the transporter within the endomembrane system (Fig. 5). Such a finding is highly interesting. It was previously known that IRT1 is post-translationally

Journal of Cell Science (2024) 137, jcs263645. doi:10.1242/jcs.263645

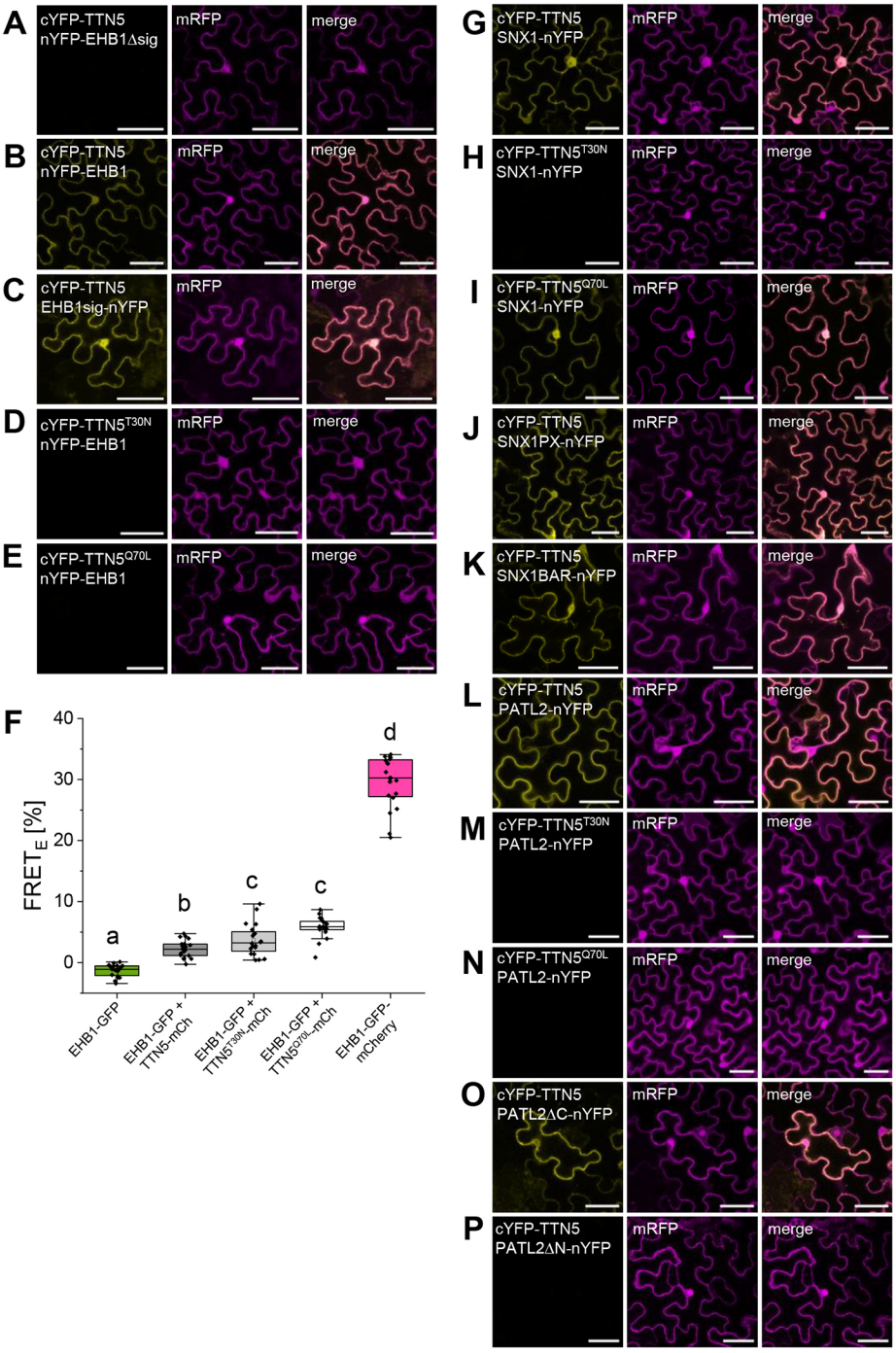

Fig. 4. TTN5 interacts with IRT1 regulators EHB1, SNX1 and PATL2. (A–E,G–P) BiFC of split YFP experiments with TTN5 and the known IRT1 regulators EHB1 (Khan et al., 2019), SNX1 (Ivanov et al., 2014) and PATL2 (Hornbergs et al., 2023). mRFP expression serves as a transformation control. (A–E) TTN5 interacts with EHB1 via the sig domain. (B) TTN5 and EHB1 showed complementation whereas (D,E) variants were not able to complement split-YFP. (A,C) TTN5 was tested together with EHB1sig (signature domain, sig domain only) and with EHB1 harboring a deletion of the CAR sig domain [sig domain as defined in Rodriguez et al. (2014), Khan et al. (2019), EHB1Δsig]. Deletion of the sig domain resulted in loss of complementation. (F) Interaction between EHB1–GFP (donor) with TTN5–mCherry and TTN5–mCherry variants (acceptor) was confirmed by FRET-APB. EHB1–GFP was used as the donor-only sample (negative control); EHB1–GFP-mCherry was used for intra-molecular FRET (positive control). In this assay, TTN5 variants interacted with EHB1. Each combination was tested a minimum of three times with 20 individual measurements (n=20) with comparable results. The box represents the 25–75th percentiles, and the median is indicated. The whiskers show the 5–95th percentiles. (G–K) BiFC showing that TTN5 interacts with SNX1. (G) TTN5 and (I) $TTN5^{Q70L}$ showed complemented YFP signal together with SNX1. No YFP fluorescence was detectable for (H) $TTN5^{T30N}$ with SNX1. (J,K) An interaction took place between TTN5 and the (J) PX and (K) the BAR domain of SNX1. (L–P) BiFC showing that TTN5 interacted with PATL2. (L) PATL2 showed complemented YFP signal with N-terminally-tagged TTN5. (M) $TTN5^{T30N}$ and (N) $TTN5^{Q70L}$ did not complement YFP with PATL2. (O,P), Deletion mutants of PATL2 showed dependency of the N-terminus for complementation with TTN5. (O) YFP signal was visible for PATL2 N-terminus (PATL2ΔC). (P) By contrast, the C-terminus alone (PATL2ΔN) had no detectable YFP. Every construct was tested a minimum of three times (n≥3) with similar results. Scale bar: 50 µm. One-way ANOVA with Tukey post-hoc test was performed. Different letters indicate statistical significance between the groups (P<0.05).

controlled through a mechanism involving the vesicular trafficking system, but components that might bind with IRT1 during this process had remained obscure. Moreover, the connections of small GTPases, like TTN5, with endomembrane trafficking were mostly not ascribed to concrete physiological roles. Hence, our report is very timely, and highlights direct protein connections between cargo and vesicle trafficking components that fills a gap in our understanding.

TTN5, an endomembrane system protein, targets IRT1vr

The protein interaction between TTN5 and IRT1 is supported by multiple findings. First, the interaction was detected in a Y2H screen, which yielded only few interaction partners, all of which could all be validated (Khan et al., 2019; Hornbergs et al., 2023). Second, the interaction was verified by using independent methods [targeted Y2H, BiFC, FRET-APB and co-immunoprecipitation (co-IP) experiments]. Third, fluorescence signals of mCherry–TTN5 and IRT1–GFP reporter proteins colocalized in cells, and their localization overlapped in intracellular membrane-associated locations in cells of the root epidermis, in which both genes are expressed. Furthermore, TTN5 was found to interact with proteins of the IRT1vr environment (Fig. 5A,B). These findings altogether indicate that, in plant roots, TTN5 and IRT1 can indeed interact in root epidermis cells in locations related to Fe acquisition. The previously described TTN5 localization pattern in vesicles and at the plasma membrane (Mohr et al., 2024) was confirmed upon colocalization with IRT1 in this study. Hence, IRT1 localization

Journal of Cell Science (2024) 137, jcs263645. doi:10.1242/jcs.263645

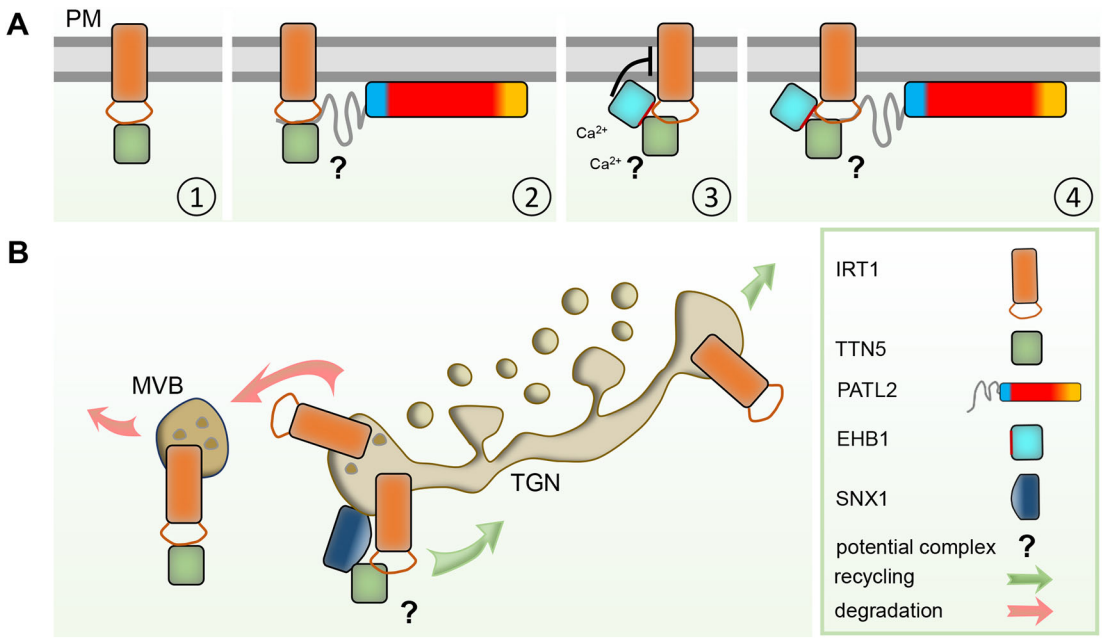

Fig. 5. Summary model of the action of TTN5 within the IRT1-regulatory network. A schematic overview of the identified TTN5 interactors within the IRT1-regulatory network (A) at the plasma membrane (PM) or (B) in the endomembrane compartments of the TGN or MVB. IRT1 undergoes a constant cycling due to endocytosis from the plasma membrane and either degradation via the lytic pathway in the vacuole or recycling back to the plasma membrane. (A) We identified TTN5 interaction with the large cytosolic variable region of IRT1. TTN5 and IRT1 colocalized at the plasma membrane (1). PATL2 interacts with the large cytosolic variable region of IRT1 (IRT1vr) via its N-terminus and might be involved in α-tocopherol recruitment to the membrane, to prevent lipid peroxidation induced by IRT1-related Fe import (Hornbergs et al., 2023). TTN5 also interacts with the N-terminus of PATL2. A potential TTN5–PATL2–IRT1 complex formation is suggested (2). EHB1 interacts with the large cytosolic variable region of IRT1 via its signature (sig) domain and inhibits IRT1 function at the plasma membrane in a Ca^{2+}-dependent manner (Khan et al., 2019). TTN5 also interacted with EHB1 via the sig domain. A potential TTN5–EHB1–IRT1 complex formation is suggested (3). A quadruple complex of IRT1, TTN5, PATL2 and EHB1 (4) is also possible. (B) We found that IRT1 colocalized with SNX1 (Ivanov et al., 2014) and TTN5 in the TGN. IRT1 and TTN5 also colocalized in MVBs. The protein representations are explained in the key; a potential protein complex that might form is indicated by a question mark.

dependent on endomembrane trafficking might be linked with the presence of TTN5 in this process.

A very interesting finding was that the mCherry–$TTN5^{T30N}$ variant tended to have higher colocalization levels at the plasma membrane with IRT1–GFP than did wild-type TTN5. This could explain previous colocalization data where an MVB marker was found to overlap more with YFP–TTN5 and the hydrolysis impaired mutant YFP–$TTN5^{Q70L}$ than YFP–$TTN5^{T30N}$ (Mohr et al., 2024), and reinforces our suggestion that TTN5 has functions in vesicle trafficking. Although a GEF is not needed for nucleotide exchange of TTN5 (Mohr et al., 2024), $TTN5^{T30N}$ might have a conformation that facilitates binding of a GEF so that $TTN5^{T30N}$, along with IRT1, might be retained at the plasma membrane by the unknown TTN5-interacting GEF. The presence of mCherry–TTN5 signals together with IRT1–GFP in wortmannin-induced swollen structures, probably indicating MVBs, supports the idea of a role in transporter degradation. MVBs are known to be the final step before vacuolar degradation (Kolb et al., 2015; Arora and Van Damme, 2021). This could indicate that the presence of TTN5 is crucial point for the IRT1 sorting fate. We therefore propose a role of TTN5 in targeting intracellular IRT1 protein (Fig. 5B). In such a process, TTN5 could be present at the plasma membrane in a resting state. After GTPase activation, it could then be recruited to the place of action, and active TTN5 would play a role in IRT1 cycling. TTN5 is thought to predominantly bind GTP and be in an active state in the cell (Mohr et al., 2024). Furthermore, there is support for a role of TTN5 in IRT1 recycling through the binding of TTN5 and SNX1. SNX1 is involved in the recycling of IRT1 at these sites (Ivanov et al., 2014). Hence, TTN5 might be in a functional complex with SNX1 to control the recycling of the cargo protein IRT1.

The observed roles of TTN5 fit well with the general understanding of ARF signaling in plasma membrane protein trafficking. The auxin transporters PIN1 and PIN2 and the boron transporter BOR1, like IRT1, are polarly localized in the plasma membrane and undergo a constant degradation-recycling process (Benková et al., 2003; Takano et al., 2010; Barberon et al., 2014). Apart from vesicle formation, as described for ARF1 or SAR1, a role in this process has been shown for other regulatory mechanisms of ARF signaling through the GEFs and GAPs (Nielsen, 2020). GNOM and BIG5, two ARF GEFs and ARF1 regulators, are described to be involved in the correct localization of the plasma membrane transporter PIN1, functioning at different regulatory steps (Geldner et al., 2003; Anders et al., 2008; Kleine-Vehn et al., 2008; Tanaka et al., 2009). In addition, another ARF GTPase, ARF1A1C, might not only partially colocalize with GNOM, but modified activity also results in impaired localization of PIN1 to the plasma membrane and also altered vacuolar targeting of PIN2 (Tanaka et al., 2014). BOR1 plasma membrane localization depends on GNOM as well (Yoshinari et al., 2021), showing that there is a good connection between ARF GEFs and plasma membrane protein localization.

Taken together, TTN5, which is an endomembrane system protein (Mohr et al., 2024) is linked with a transporter protein whose abundance is controlled by endomembrane trafficking. For future studies, stable coexpression of both proteins under the control of their endogenous promoters will be needed to investigate the effect of TTN5 on IRT1 localization. Finally, owing to the very low intrinsic GTP hydrolysis activity of TTN5, identification of TTN5 GAPs will shed light on TTN5 function in Fe homeostasis and

Journal of Cell Science (2024) 137, jcs263645. doi:10.1242/jcs.263645

potentially other cellular signaling events. It will also be interesting to explore whether a membrane-localized GEF exists that can act upon TTN5. Future identification of potential TTN5 GEF and GAP proteins will be of great interest to clarify the role of TTN5 in endomembrane trafficking with particular reference to cues controlling IRT1.

TTN5 might play a general role in Fe nutrition

TTN5 does not only have an influence on IRT1 but also on other aspects in Fe nutrition. A partial lack of TTN5 results in decreased Fe reductase activity. The decrease in Fe reductase activity is likely caused by an effect on FRO2. It has been shown that IRT1 can interact with FRO2 to form a complex for a highly effective Fe uptake machinery (Martín-Barranco et al., 2020). Reduced Fe reductase activity could be due to an indirect influence of TTN5 on the complex formation or it could be directly driven by TTN5. Interestingly, both *ehb1* and *patl2* seedlings have a higher Fe reductase activity under Fe deficiency compared to what is seen in wild-type plants (Khan et al., 2019; Hornbergs et al., 2023). If EHB1 and PATL2 also act on FRO2, this points to an opposing role of TTN5 on the Fe deficiency response in the protein complex. Gene expression analysis revealed no great impact on Fe-related genes in *ttn5-1*$^{+/-}$ roots, implying that the effect of TTN5 is mostly at the posttranslational level.

It is a possibility that TTN5 has very different effects depending on its localization in the cell. For example, the effect on Fe reduction could be different from its effect on colocalization with IRT1 in MVBs. Different types of interaction partners have been reported for the human ARL2 with connection to distinct cellular functions in tubulin folding and microtubule dynamics (Bhamidipati et al., 2000) or in mitochondria (Sharer et al., 2002). Based on these distinct locations and the associated functions of ARL2, it has been proposed that ARL2 might act at a high level in signaling (Francis et al., 2016). This might be also the case in *Arabidopsis*. For example, TTN5 might bridge TTN5 microtubule function (Mayer et al., 1999) with IRT1 regulation.

TTN5 interacts with EHB1, SNX1 and PATL2 and might coordinate IRT1 regulation

The close interaction of TTN5 with EHB1 was suggested by BiFC and FRET-APB, and with PATL2 and SNX1 by BiFC. The interactions are further supported by deletion mutant approaches. Moreover, the interacting sites of PATL2 and EHB1 with TTN5 are similar to those for IRT1vr, again supporting the possibility that these domains and motifs are at the basis of a protein complex forming at the IRT1vr regulatory platform.

The interaction of TTN5 with the IRT1 regulators EHB1, PATL2 and SNX1 suggests that it could not only be linked with Fe nutrition but also the associated Ca^{2+} and reactive oxygen species (ROS) signaling events (Khan et al., 2019; Hornbergs et al., 2023). EHB1 is additionally interesting as a member of the CAR family. Several CAR proteins can initiate Ca^{2+}-dependent membrane curvature, which might provide a direct link to vesicle trafficking. Interestingly, Ca^{2+} is bound by EHB1 via its C2 domain, which is also a common feature of class III ARF GAPs (Vernoud et al., 2003; Knauer et al., 2011). Indeed, EHB1 is directly linked to ARF signaling in an antagonistic interaction with the ARF GAP AGD12 in gravitropic bending (Dümmer et al., 2016; Rath et al., 2020). Further research is needed to investigate whether TTN5 can also interact with the C2-domain containing ARF GAPs AGD11 and AGD13. Additionally, crystallization experiments have revealed a potential Ca^{2+}-binding site between HsARF6 and its GAP ASAP3. The GTP hydrolysis was stimulated in the presence of Ca^{2+}, suggesting that there is a link between Ca^{2+} and ARF signaling (Ismail et al., 2010). We therefore consider the possibility that the interaction between TTN5 and EHB1 occurs in a Ca^{2+}-dependent manner. PATL2 might interact with IRT1 to prevent lipid peroxidation stress (Hornbergs et al., 2023). Prolonged Fe deficiency leads to an increase in hydrogen peroxide concentration as well as an activity increase of catalase CAT2 (Le et al., 2015; von der Mark et al., 2020; Gratz et al., 2021). Some catalases are present in the PATL2 interactome in roots (Hornbergs et al., 2023). Future studies should address whether TTN5 is connected with oxidative stress and Ca^{2+} signaling.

SNX1 is a positive regulator for IRT1 recycling to the plasma membrane in the sorting endosomes (Ivanov et al., 2014) and for endosomal recycling of the auxin efflux carrier PIN2 (Jaillais et al., 2006). SNX1 is therefore part of the system that mediates recycling of specific plasma membrane proteins. Interestingly, deficiency of BLOS1 leads to accumulation of PIN1 and PIN2 at the plasma membrane (Cui et al., 2010). BLOS1 seems to be an ortholog of the mammalian biogenesis of lysosome-related organelles complex 1 (BLOC-1), which is responsible for vesicle transport from endosomes to lysosomes (Li et al., 2007; Raposo et al., 2007). SNX1 can interact with both BLOS1 and BLOS2, and could therefore also play a role in vesicle-mediated transport through these interactions (Cui et al., 2010; Heucken and Ivanov, 2018). SNX1 possesses a BAR domain, which is also typical for class I ARF GAPs (Vernoud et al., 2003; Heucken and Ivanov, 2018). A connection between the SNX1 BAR domain and an ARF6 GEF has been identified in mouse by their interaction. This interaction was associated with a positive effect of ARF6 function (Fukaya et al., 2014), and colocalization analysis revealed overlapping expression in endosomes, which fits the known SNX1 localization in *Arabidopsis* (Fukaya et al., 2014; Ivanov et al., 2014), so this could be a possible interconnection between ARF signaling and SNX1. Here, we identified an interaction between TTN5 and SNX1, which could be the crucial link in the decision between SNX1-dependent recycling and degradation of IRT1. SNX1 could be needed for a potential TTN5 GEF and subsequent recruitment of TTN5 to membranes. Based on the opposing roles of EHB1 and SNX1 in IRT1 regulation, and their connection to TTN5, we suggest a coordinating role for TTN5 in transporting IRT1 between plasma membrane and endosomes by interacting with peripheral membrane proteins such as EHB1, PATL2 and SNX1. The findings that some ARF GAPs have a C2 or BAR domain, and that SNX1 interacts with an ARF GEF, strengthen the interest in the identification of TTN5 GEFs and GAPs.

Further research has to focus on physiological aspects in either combined knockout mutants or tagged-protein lines to arrange and decipher the IRT1 regulatory network. An intriguing open question is whether a large IRT1vr–EHB1–PATL2–TTN5–SNX1 complex is assembled. If so, the next question is how, when and in which order the individual or all components of the IRT1vr complex are assembled. Another question is what the structural requirements for proper protein conformations and membrane interfaces are (Fig. 5A,B).

Conclusion and perspectives

This study provides hints that the ARF-like GTPase TTN5 contributes to endocytosis and vesicle trafficking of IRT1 by way of a protein complex at IRTvr comprising TTN5 and other IRT1 interactors. Evidence that small GTPases can bind with plasma membrane and peripheral membrane proteins is instrumental to understanding how membrane proteins are controlled by vesicular trafficking components in plants. An intriguing question is whether TTN5 also targets other transmembrane cargo proteins. Future work might uncover additional functions of TTN5 or of other GTPase protein complexes of this kind

and determine the requirements and order of events for complex assembly leading to vesicular trafficking.

MATERIALS AND METHODS

Yeast two-hybrid screen

The Y2H screen for identification of IRT1vr interactors was performed previously and is described in Khan et al. (2019). Targeted Y2H interactions were tested using the GAL4 transcription factor system with histidine as selection marker. The *TTN5* coding sequence was amplified using TITAN5 nter B1 and TITAN5 stop B2 primers (for primer sequences, see Table S1). Obtained fragments were cloned into pDONR207 via Gateway BP reaction (Life Technologies) with following LR reactions into pGBKT7-GW (binding domain, BD) or pACT2-GW (activation domain, AD). Both vectors were a kind gift from Dr Yves Jacob (Institut Pasteur, Paris, France). The yeast strain AH109 was co-transformed with the corresponding AD- and BD-tagged expression vectors. The combination pACT2:SNX1 and pGBKT7:SNX1 (Pourcher et al., 2010) was used as a positive control. Negative controls were co-transformations with the respective non-recombined pACT2-GW or pGBKT7-GW. Drop tests were performed with synthetic defined (SD) –Leu, –Trp medium (Takara Bio) cultures at an optical density at 600 nm (OD_{600}) of 0.1 and three additional 1:10 dilution steps (10^1-10^4) on SD –Leu, –Trp and SD –Leu, –Trp, –His with 0.5 mM 3-amino-1,2,4-triazole plates. One of each plate was incubated either at 30°C or at room temperature, wrapped in aluminum foil, for up to 2 weeks. The experiment was performed three times.

N. benthamiana leaf infiltration

N. benthamiana plants were grown on soil for 2–4 weeks in a greenhouse facility under long-day conditions (16 h light, 8 h darkness, 20°C). *N. benthamiana* leaf infiltration was performed with the Agrobacterium (*Rhizobium radiobacter*) strain C58 (GV3101; kind gift from Jörg Kudla, University of Münster, Germany) carrying the respective constructs for confocal microscopy. Agrobacteria cultures were grown overnight at 28°C, centrifuged for 5 min at 4°C at 5000 ***g***, resuspended in infiltration solution (5% sucrose, a pinch of glucose, 0.01% Silwet Gold, 150 µM acetosyringone) and incubated for 1 h at room temperature. Bacterial suspension was set to an OD_{600}=0.4 and infiltrated into the abaxial side of *N. benthamiana* leaves.

Expression of pABind and pMDC7 (Curtis and Grossniklaus, 2003; Bleckmann et al., 2010) constructs was induced with a β-estradiol solution (20 µM β-estradiol and 0.1% Tween 20) 16 h before imaging.

Bimolecular fluorescence complementation

BiFC was used to study protein interaction of TTN5 and the respective GTPase $TTN5^{T30N}$ and $TTN5^{Q70L}$ variants with other proteins in plant cells. At first, entry clones were generated. *TTN5*, $TTN5^{T30N}$ and $TTN5^{Q70L}$ coding sequences with a stop codon were amplified using the primers TITAN5 n-ter B1 and TITAN5 stop B4 (Table S1). The *IRT1vr* coding sequence with a stop codon was amplified using the primers I1L1B3 and I1LB2. For amplifying full-length *EHB1*, the primer pair EHB1 n-ter B3 and EHB1 stop B2 was used. Amplification of *EHB1Δsig* is described in Khan et al. (2019). The *SNX1* coding sequence without stop codon for C-terminal fusion was amplified using the primer SNX1 B3 and SNX1ns B2. Cloning of SNX1 deletion mutants SNX1PX and SNX1BAR was done using the primers SNX1 B3 and PXSNX1 rev and BARSNX1 fwd and SNX1ns B2 respectively. The used PATL2 constructs are described in Hornbergs et al. (2023). The amplified PCR products were cloned via Gateway BP reaction (Life Technologies) into pDONR221-P1P4 (Invitrogen) or pDONR221-P3P2 (Invitrogen).

The obtained constructs were then used to prepare final recombinant destination vectors in an LR reaction (Life Technologies) for cloning into pBiFCt-2in1 vectors (Grefen and Blatt, 2012). Agrobacteria were transformed with correct constructs and used for *N. benthamiana* leaf infiltration. After 48 h, the mRFP expression control signal and YFP signals were detected by fluorescent microscopy (LSM 780, Zeiss) with a 40× C-Apochromat water immersion objective. YFP constructs were detected at 491–560 nm after exciting at 488 nm, and mCherry fluorescence was excited at 561 nm and emission detected at 570–633 nm.

The BiFC constructs were tested in three independent replicates with three infiltrated leaves each. The vectors pBiFC-2in1-NN and pBiFC-2in1-CN were kindly provided by Dr Christopher Grefen, Tübingen, Germany.

Förster-resonance-energy transfer acceptor photo bleaching

FRET-APB was used to verify protein–protein interactions of TTN5 $TTN5^{T30N}$, and $TTN5^{Q70L}$. The coding sequences without a stop codon were amplified with the primers TITAN5 B1 and TITAN5 ns B2 (Table S1), and cloned into the pDONR207 (Invitrogen, BP reaction, Life Technologies). Cloning of pDONR207:IRT1vr and pDONR207:EHB1 is described in Khan et al. (2019). The obtained constructs were used for LR reactions (Life Technologies) with the pABind-GFP, pABind-mCherry and pABind-FRET for C-terminal tagging (Bleckmann et al., 2010). N-terminal GFP–TTN5 constructs were cloned by overlap extension PCR simultaneously with mCherry–TTN5 constructs (see section 'Subcellular localization of fluorescent protein fusions' below). In the first step, the primer pairs GFP B1 with GFP R ns BIND and GFP to TTN5 with TITAN5 stop B2 were used with pABind-FRET (Bleckmann et al., 2010) as template for the fluorescent protein coding sequence. The final construct was obtained with the primer pair GFP B1 with TITAN5 stop B2. Constructs were cloned into pDONR207 for further cloning into pMDC7 via LR reactions. Agrobacteria were transformed and used for *N. benthamiana* leaf infiltration. FRET-APB was performed using laser-scanning confocal microscopy (LSM 780, Zeiss) with a 40× C-Apochromat water immersion objective. GFP was excited at 488 nm and detected at 491–560 nm, and mCherry fluorescence was excited at 561 nm and detected at 570–633 nm. GFP and mCherry channels were recorded for five scans. The mCherry signal was then bleached with 70 iterations of maximum laser intensity in a specific region of interest (ROI) which was set to the nucleus. Both channels were detected for additional 20 post-bleaching scans. FRET-APB measurements were performed with a minimum of 10 repetitions ($n \geq 10$).

Arabidopsis plant material

The *Arabidopsis ttn5-1* mutant was previously described (McElver et al., 2000). Heterozygous seedlings were selected by PCR on gDNA using the primer TTN5 intron1 fwd and pDAP101 LB1 (Table S1). pro35S::YFP-TTN5 and pro35S::HA_3-TTN5 lines were previously described (Mohr et al., 2024) as were proIRT1::IRT1-mCitrine/*irt1-1* (Dubeaux et al., 2018). *irt1-1* (Ws) was characterized in Vert et al. (2002) and *irt1-1* (Col-0, SALK_054554) in Fukao et al. (2011).

Reporter lines were constructed as follows: proIRT1::IRT1-mCherry, with the mCherry at position 80 in the first cytoplasmic loop, was cloned by overlap-extension PCR. *mCherry* was amplified from pABind:mCherry (Bleckmann et al., 2010) using primer pair link mCh F and mCh ns link R. IRT1 halves were amplified using IRT1 B1 and IRT1Q80 link R and link IRT1Q80 F and IRT1 stop B2. In a final PCR, IRT1–mCherry was amplified with primer pair IRT1 B1 and IRT1 stop B2. BP and LR reaction (Life Technologies) were performed as described above with pIM5 as the destination vector. The Gateway-suitable plasmid pIM5 was created by exchanging pro35S from pMCD32 with proIRT1 using AQUA cloning (Beyer et al., 2015). The IRT1 promoter was amplified from gDNA using primer pair pIM5-pIRT1 F and pIM5-pIRT1 R with pMDC32-complementary overhangs and the restriction sites HindIII and KpnI, respectively. The IRT1–GFP construct, with the GFP at position 173 in the variable cytoplasmic loop, was cloned by overlap-extension PCR. *GFP* was amplified from pABind:GFP (Bleckmann et al., 2010) using primer pair IG173 F and GI173 R. IRT1 halves were amplified using IRT1 B1 and IG173 R and GI173 R and IRT1 stop B2. In a final PCR, IRT1–GFP was amplified with primer pair IRT1 B1 and IRT1 stop B2. BP and LR reaction were performed as described above with pMDC32 (Curtis and Grossniklaus, 2003) as destination vector. Agrobacterium cultures containing the plant protein expression vectors, generated as described above, were used for floral dip transformation of *Arabidopsis*. Plants were multiplied, PCR-genotyped using specific primer pairs (Table S1) and selected according to standard procedures.

Co-immunoprecipitation and pulldown experiments

Immunoprecipitation (IP) was performed with *Arabidopsis* seedlings grown for 10 days under Fe-deficient conditions. Plants with proIRT1::IRT1-

Journal of Cell Science (2024) 137, jcs263645. doi:10.1242/jcs.263645

mCherry in either the HA_3–TTN5 or wild-type background were grown and analyzed in parallel. Approximately 60 seedlings were flash-frozen in liquid nitrogen and ground using the Retsch MM200 with cooled grinding jars in the presence of two metal balls for 2 min. Ground material was solubilized in 1 ml IP buffer (50 mM Tris-HCl pH 8, 150 mM NaCl, 1 mM EDTA, 1% Triton X-100 and cOmpete Mini Protease Inhibitor). The solution was incubated for 10 min at room temperature followed by a 10 min centrifugation at 4°C and 17,000 ***g*** (maximum speed). The supernatant was transferred into a fresh 1.5 ml reaction tube. The centrifugation step was repeated until all cellular debris were removed and 50 µl was taken as the crude extract (CE) aliquot. Next, 25 µl anti-HA magnetic beads (Thermo Fisher Scientific, Pierce) were added to the solution and the reaction was incubated overnight at 4°C while rotating. A magnet was used to collect the beads at the side of the reaction tube and solution was transferred to a fresh 1.5 ml reaction tube (Flow through). Then, 1 ml IP buffer was added to wash beads (Wash I). The collection of the supernatant and washing procedure was repeated twice. proIRT1::IRT1-mCherry immunodetection was performed using primary anti-RFP antibody (rabbit, 1:1000, abcam, ab62341) and secondary anti-rabbit-IgG conjugated to HRP antibody (goat, 1:5000, Agrisera, AS09 602). Immunodetection of HA_3–TTN5 was conducted using an anti-HA–HRP antibody (rat, 1:1000, Roche, clone 3F10, 11867423001). IP was performed twice in two replicates each (n=2).

Arabidopsis physiological Fe deficiency growth experiments

Arabidopsis seeds were sterilized with sodium hypochlorite solution (6% Sodium hypochlorite and 0.1% Triton X-100) and stored 24 h at 4°C for stratification. Seedlings were grown upright on Hoagland medium [1.5 mM $Ca(NO_3)_2$, 0.5 mM KH_2PO_4, 1.25 mM KNO_3, 0.75 mM $MgSO_4$, 1.5 µM $CuSO_4$, 50 µM H_3BO_3, 50 µM KCl, 10 µM $MnSO_4$, 0.075 µM $(NH_4)_6Mo_7O_{24}$, 2 µM $ZnSO_4$ and 1% sucrose, pH 5.8, supplemented with 1.4% Plant agar (Duchefa)] with sufficient (50 µM FeNaEDTA, +Fe) or deficient (0 µM FeNaEDTA, –Fe) Fe supply in growth chambers (CLF Plant Climatics) under long-day conditions (16 h light at 21°C, 8 h darkness at 19°C). Seedlings were grown on Fe-sufficient or -deficient medium for 6 or 10 days or in a 2-week growth system with plants growing 14 days on Fe-sufficient medium and then being transferred to either fresh Fe-sufficient or Fe-deficient medium for an additional 3 days.

Root length

For root length comparison, plants were growing for 10 days in Fe-sufficient or -deficient conditions and photographed including a scale ruler in the picture. Root lengths were measured from root tip to hypocotyl using the JMicro Vision program (https://jmicrovision.github.io) (+Fe: WT n=19; *ttn5-1* n=28; –Fe: WT n=16; *ttn5-1* n=32).

Chlorophyll content

For chlorophyll content comparison, plants were grown in the 2-week system in Fe-sufficient or -deficient conditions. Chlorophyll content was measured by SPAD values using SPAD-502plus (Konica Minolta Optics, 2012) with up to ten biological replicates (+Fe: n=10; –Fe: n=9). Chlorophyll content was determined in three individual experiments.

ttn5-1 phenotyping on alkaline calcareous soil

Sterilized seeds were placed on Fe-sufficient Hoagland plates in three rows with 12–15 seeds, stratified at 4°C in darkness for 3 days and then [on the day of sowing (DAS)] grown upright for 9 days. A total of 16 wild-type and 16 *ttn5-1*$^{+/-}$ seedlings were selected for transfer onto two soil conditions, control and alkaline calcareous soil (ACS). The control condition consisted of peat-based soil (Floraton 1, Floragard, Oldenburg, Germany), 20 g vermiculite (Agrivermiculite Floragard, Oldenburg, Germany) and 400 ml distilled water per liter dry soil. The ACS soil additionally contained 8 g $CaCO_3$ (AppliChem, Darmstadt, Germany) and 4 g $NaHCO_3$ (Fisher Scientific, Hampton, USA). The pH in water (1:10 soil:water) was 6.2 for the control soil and 8.0 for the ACS soil 30 min after mixture. The soil was filled into 7 cm×7 cm×6.5 cm pots (Pöppelmann GmbH & Co. KG Kunststoffwerk–Werkzeugbau, Lohne Germany) and afterwards 7.5 cm×7.5 cm large squares of ultramarine blue plotter foil (Europe Warehouse GmbH & Co. KG, Wuppertal, Germany) were stuck on the pots. Seedlings were then planted into 1 cm diameter round holes in the foil. Eight plants were grown per soil and condition. After 1 week, the 1 cm holes were closed around the seedlings.

Plants were watered for 1 week with deionized water. Then control plants were watered with deionized water and ACS plants with 20 g/l $NaHCO_3$ (second week) and 25 g/l $NaHCO_3$ (following weeks). At 28 days after sowing the plants were scanned with a PlantEye MicroScan (Phenospex, Heerlen, The Netherlands), a multispectral scanner determining positions and color of points using a laser and four additional wavelengths (red, 624–634 nm; green, 530–540 nm; blue, 465–485 nm; and near-infrared, 720–750 nm). By filtering out the blue color (hue 200–360) from the images the background around the plants was removed from the measurements. Each plant was scanned twice, and the average of the technical replicates was calculated. The parameter '3D leaf area' and 'normalized differential vegetation index' (NDVI) average were determined with the PlantEye MicroScan according to the instruction manual, corresponding to an approximation of aerial plant biomass and chlorophyll content. Photos of the plants were acquired with a camera (α 600, Sony, Tokyo, Japan). The entire experiment was conducted once with n=8.

Gene expression analysis by RT-qPCR

For gene expression analysis, plants were grown in the 2-week system. Total RNA was isolated from roots using the RNeasy Mini Kit (Qiagen) and cDNA synthesis was performed with the RevertAid RT Reverse Transcription Kit (Thermo Fisher Scientific). The CFX96 Touch™ Real-Time PCR Detection System (Bio-Rad) was used for RT-qPCR performance. Data processing was undertaken with Bio-Rad CFX Manager™ (version3.1) software. Mass standard curve analysis was used for determination of the absolute gene expression and the elongation factor *EF1Bα* expression served as a reference for normalization. RT-qPCR was performed in three biological replicates (n=3) and two technical replicates each. All primer pairs used in this study are listed in Table S1.

Fe reductase activity assay

Fe reductase activity assay was performed as described previously (Gratz et al., 2019). For Fe reductase activity, plants were grown in the 2-week system in Fe-sufficient or -deficient conditions. Two plants per replicate were washed in 100 mM $Ca(NO_3)_2$, then incubated for 1 h in the dark in 1.5 ml Fe reductase solution (300 mM ferrozine and 100 mM FeNaEDTA). The Fe reductase activity-dependent color change was measured at 562 nm using an Infinite 200® PRO (Tecan) plate reader. The activity calculation was undertaken using the ferrozine extinction coefficient ε=28.6 mM^{-1} cm^{-1} and was normalized to root weight. The assay was performed with a minimum of three replicates (n≥3), each consisting of a pool of two plants. Fe reductase activity was determined in three individual experiments.

Subcellular localization of fluorescent protein fusions and microscopy

The creation of $TTN5^{T30N}$ and $TTN5^{Q70L}$ constructs by introduction of point mutations and generation of pro35S::YFP-TTN5 is described in Mohr et al. (2024). mCherry-tagged constructs were created by overlap-extension PCR. Fluorescent protein was amplified from pABind:mCherry (Bleckmann et al., 2010) using primer pair mCherry B1 and mCh R ns BIND. *TTN5*, $TTN5^{T30N}$ and $TTN5^{Q70L}$ CDS were amplified with a 20 bp overlap of mCherry using mCh to TTN5 and TITAN5 stop B2. In a third PCR mCherry-tagged TTN5 constructs were generated with the mCherry B1 and TITAN5 stop B2 primer pair. The BP and LR reaction was performed as described above. The XVE-driven β-estradiol inducible vector pMDC7 (Curtis and Grossniklaus, 2003) was chosen as destination vector. Cloning of IRT1–GFP is described above (see section '*Arabidopsis* plant material'). The IRT1–mCherry construct is described in Ivanov et al. (2014) and proIRT1::IRT1-mCitrine/*irt1-1* in Dubeaux et al. (2018). Agrobacteria were transformed with the obtained constructs and tested by *N. benthamiana* leaf infiltration after 2 days of expression.

Localization studies were carried out by laser-scanning confocal microscopy (LSM 780, Zeiss) with a 40× C-Apochromat water immersion objective. YFP constructs were excited at 488 nm and detected at 491–560 nm. mCherry or FM4-64 fluorescence was excited at 561 nm

and detected at 570–633 nm. Each combination was tested a minimum of three times ($n \geq 3$).

Wortmannin (10 µM, Sigma-Aldrich) and plasma membrane dye FM4-64 (165 µM, Thermo Fisher Scientific) were infiltrated into *N. benthamiana* leaves. FM4-64 was detected after 5 min incubation and wortmannin was incubated for 25 min before checking the treatment effect.

JACoP-based colocalization analysis

Colocalization analysis was performed with the ImageJ (Schneider et al., 2012) plugin 'Just Another Colocalization Plugin' (JACoP) (Bolte and Cordelières, 2006). A comparison of Pearson's and overlap coefficients was undertaken. Object-based analysis was performed for spotted-structures, as adapted from the process described in Ivanov et al. (2014). The percentage of colocalization for both channels was calculated based on distance between geometrical centers of signals. Analysis was conducted in three replicates each (n=3).

Statistical analysis

One-way ANOVA was used for statistical analysis and performed in OriginPro 2019. Fisher LSD or Tukey was chosen as the post-hoc test with $P<0.05$.

Accession numbers

Sequence data from this article can be found in the TAIR and GenBank data libraries under accession numbers: *FRO2* (TAIR: AT1G01580), *EHB1* (TAIR: AT1G70800), *IRT1* (TAIR: AT4G19690), *PATL2* (TAIR: AT1G22530), *TTN5* (TAIR: AT2G18390) and *SNX1* (TAIR: AT5G06140).

Acknowledgements

We thank Gintaute Matthäi and Elke Wieneke for excellent technical assistance. We thank Ksenia Trofimov for microscopic help and advice, and Rubek Merina Basgaran for help with protein interaction studies. We are thankful for the excellent assistance from Stefanie Weidtkamp-Peters and Sebastian Hänsch, members of the Center for Advanced Imaging (CAi) at the Heinrich Heine University. Funding for instrumentation was from Zeiss LSM780: DFG- INST 208/551-1 FUGG.

Competing interests

The authors declare no competing or financial interests.

Author contributions

Conceptualization: I.M., P.B., R.I.; Formal analysis: I.M., P.B., R.I.; Funding acquisition: P.B.; Investigation: I.M., M.E., M.C.K., N.S., R.G., K.A., L.G., T.B., R.I.; Supervision: I.M., T.B., P.B., R.I.; Writing – original draft: I.M.; Writing – review & editing: P.B., R.I.

Funding

This work was supported by the Deutsche Forschungsgemeinschaft (DFG, German Research Foundation), SFB 1208 project B05 to P.B. This work received funding by Deutsche Forschungsgemeinschaft (DFG, German Research Foundation) under Germany's Excellence Strategy – EXC-2048/1 – project ID 390686111 and – TRR 341/1 – Project ID 456082119. Open access funding provided by Heinrich-Heine-Universität Düsseldorf. Deposited in PMC for immediate release.

Data availability

Raw microscopic image data are available via BioImage Archive (https://www.ebi.ac.uk/bioimage-archive/) with the accession number S-BIAD1351 (doi:10.6019/S-BIAD1351).

Peer review history

The peer review history is available online at https://journals.biologists.com/jcs/lookup/doi/10.1242/jcs.263645.reviewer-comments.pdf

References

Adarska, P., Wong-Dilworth, L. and Bottanelli, F. (2021). ARF GTPases and their ubiquitous role in intracellular trafficking beyond the golgi. *Front. Cell Dev. Biol.* **9**, 679046-679046. doi:10.3389/fcell.2021.679046

Anders, N., Nielsen, M., Keicher, J., Stierhof, Y. D., Furutani, M., Tasaka, M., Skriver, K. and Jürgens, G. (2008). Membrane association of the Arabidopsis ARF exchange factor GNOM involves interaction of conserved domains. *Plant Cell* **20**, 142-151. doi:10.1105/tpc.107.056515

Antoshechkin, I. and Han, M. (2002). The *C. elegans* evl-20 gene is a homolog of the small GTPase ARL2 and regulates cytoskeleton dynamics during cytokinesis and morphogenesis. *Dev. Cell* **2**, 579-591. doi:10.1016/S1534-5807(02)00146-6

Arora, D. and Van Damme, D. (2021). Motif-based endomembrane trafficking. *Plant Physiol.* **186**, 221-238. doi:10.1093/plphys/kiab077

Barberon, M., Zelazny, E., Robert, S., Conéjéro, G., Curie, C., Friml, J. and Vert, G. (2011). Monoubiquitin-dependent endocytosis of the IRON-REGULATED TRANSPORTER 1 (IRT1) transporter controls iron uptake in plants. *Proc. Natl Acad. Sci. USA* **108**, E450-E458. doi:10.1073/pnas.1100659108

Barberon, M., Dubeaux, G., Kolb, C., Isono, E., Zelazny, E. and Vert, G. (2014). Polarization of IRON-REGULATED TRANSPORTER 1 (IRT1) to the plant-soil interface plays crucial role in metal homeostasis. *Proc. Natl Acad. Sci. USA* **111**, 8293-8298. doi:10.1073/pnas.1402262111

Benková, E., Michniewicz, M., Sauer, M., Teichmann, T., Seifertová, D., Jürgens, G. and Friml, J. (2003). Local, efflux-dependent auxin gradients as a common module for plant organ formation. *Cell* **115**, 591-602. doi:10.1016/S0092-8674(03)00924-3

Beyer, H. M., Gonschorek, P., Samodelov, S. L., Meier, M., Weber, W. and Zurbriggen, M. D. (2015). AQUA Cloning: a versatile and simple enzyme-free cloning approach. *PLoS One* **10**, e0137652. doi:10.1371/journal.pone.0137652

Bhamidipati, A., Lewis, S. A. and Cowan, N. J. (2000). ADP ribosylation factor-like protein 2 (Arl2) regulates the interaction of tubulin-folding cofactor D with native tubulin. *J. Cell Biol.* **149**, 1087-1096. doi:10.1083/jcb.149.5.1087

Bleckmann, A., Weidtkamp-Peters, S., Seidel, C. A. M. and Simon, R. (2010). Stem cell signaling in Arabidopsis requires CRN to localize CLV2 to the plasma membrane. *Plant Physiol.* **152**, 166-176. doi:10.1104/pp.109.149930

Bolte, S. and Cordelières, F. P. (2006). A guided tour into subcellular colocalization analysis in light microscopy. *J. Microsc.* **224**, 213-232. doi:10.1111/j.1365-2818.2006.01706.x

Chen, W., Zhou, H., Xu, F., Yu, M., Coego, A., Rodriguez, L., Lu, Y., Xie, Q., Fu, Q., Chen, J., G. et al. (2023). CAR modulates plasma membrane nano-organization and immune signaling downstream of RALF1-FERONIA signaling pathway. *New Phytol.* **237**: 2148-2162. doi:10.1111/nph.18687

Cointry, V. and Vert, G. (2019). The bifunctional transporter-receptor IRT1 at the heart of metal sensing and signalling. *New Phytol.* **223**, 1173-1178. doi:10.1111/nph.15826

Connolly, E. L., Fett, J. P. and Guerinot, M. L. (2002). Expression of the IRT1 metal transporter is controlled by metals at the levels of transcript and protein accumulation. *Plant Cell* **14**, 1347-1357. doi:10.1105/tpc.001263

Cui, Y., Li, X., Chen, Q., He, X., Yang, Q., Zhang, A., Yu, X., Chen, H., Liu, N., Xie, Q., W. et al. (2010). BLOS1, a putative BLOC-1 subunit, interacts with SNX1 and modulates root growth in Arabidopsis. *J. Cell Sci.* **123**: 3727-3733. doi:10.1242/jcs.069732

Cui, Y., Shen, J., Gao, C., Zhuang, X., Wang, J. and Jiang, L. (2016). Biogenesis of Plant Prevacuolar Multivesicular Bodies. *Molecular Plant* **9**, 774-786. doi:10.1016/j.molp.2016.01.011

Cui, M. G., Gupta, S. K. and Bauer, P. (2023). Role of the plant-specific calcium-binding C2-DOMAIN ABSCISIC ACID-RELATED (CAR) protein family in environmental signaling. *Eur. J. Cell Biol.* **102**, 151322. doi:10.1016/j.ejcb.2023.151322

Curtis, M. D. and Grossniklaus, U. (2003). A gateway cloning vector set for high-throughput functional analysis of genes in planta. *Plant Physiol.* **133**, 462-469. doi:10.1104/pp.103.027979

Dubeaux, G., Neveu, J., Zelazny, E. and Vert, G. (2018). Metal sensing by the IRT1 transporter-receptor orchestrates its own degradation and plant metal nutrition. *Mol. Cell* **69**, 953-964.e955. doi:10.1016/j.molcel.2018.02.009

Dümmer, M., Michalski, C., Essen, L. O., Rath, M., Galland, P. and Forreiter, C. (2016). EHB1 and AGD12, two calcium-dependent proteins affect gravitropism antagonistically in *Arabidopsis thaliana*. *J. Plant Physiol.* **206**, 114-124. doi:10.1016/j.jplph.2016.09.006

Eide, D., Broderius, M., Fett, J. and Guerinot, M. L. (1996). A novel iron-regulated metal transporter from plants identified by functional expression in yeast. *Proc. Natl. Acad. Sci. U.S.A.* **93**, 5624-5628. doi:10.1073/pnas.93.11.5624

Fansa, E. K. and Wittinghofer, A. (2016). Sorting of lipidated cargo by the Arl2/Arl3 system. *Small GTPases* **7**, 222-230. doi:10.1080/21541248.2016.1224454

Fleming, J. A., Vega, L. R. and Solomon, F. (2000). Function of tubulin binding proteins in vivo. *Genetics* **156**, 69-80. doi:10.1093/genetics/156.1.69

Francis, J. W., Turn, R. E., Newman, L. E., Schiavon, C. and Kahn, R. A. (2016). Higher order signaling: ARL2 as regulator of both mitochondrial fusion and microtubule dynamics allows integration of 2 essential cell functions. *Small GTPases* **7**, 188-196. doi:10.1080/21541248.2016.1211069

Frost, A., Unger, V. M. and De Camilli, P. (2009). The BAR domain superfamily: membrane-molding macromolecules. *Cell* **137**, 191-196. doi:10.1016/j.cell.2009.04.010

Fukao, Y., Ferjani, A., Tomioka, R., Nagasaki, N., Kurata, R., Nishimori, Y., Fujiwara, M. and Maeshima, M. (2011). iTRAQ Analysis reveals mechanisms of growth defects due to excess zinc in Arabidopsis. *Plant Physiol.* **155**, 1893-1907. doi:10.1104/pp.110.169730

Fukaya, M., Fukushima, D., Hara, Y. and Sakagami, H. (2014). EFA6A, a guanine nucleotide exchange factor for Arf6, interacts with sorting nexin-1 and regulates neurite outgrowth. *J. Neurochem.* **129**, 21-36. doi:10.1111/jnc.12524

Gaither, L. A. and Eide, D. J. (2001). Eukaryotic zinc transporters and their regulation. *Biometals* **14**, 251-270. doi:10.1023/A:1012988914300

Geldner, N., Anders, N., Wolters, H., Keicher, J., Kornberger, W., Muller, P., Delbarre, A., Ueda, T., Nakano, A. and Jürgens, G. (2003). The Arabidopsis GNOM ARF-GEF mediates endosomal recycling, auxin transport, and auxin-dependent plant growth. *Cell* **112**, 219-230. doi:10.1016/S0092-8674(03)00003-5

Gratz, R., Manishankar, P., Ivanov, R., Köster, P., Mohr, I., Trofimov, K., Steinhorst, L., Meiser, J., Mai, H. J., Drerup, M., S. et al. (2019). CIPK11-Dependent phosphorylation modulates FIT activity to promote Arabidopsis iron acquisition in response to calcium signaling. *Dev. Cell* **48**: 726-740.e710. doi:10.1016/j.devcel.2019.01.006

Gratz, R., von der Mark, C., Ivanov, R. and Brumbarova, T. (2021). Fe acquisition at the crossroad of calcium and reactive oxygen species signaling. *Curr. Opin. Plant Biol.* **63**, 102048. doi:10.1016/j.pbi.2021.102048

Grefen, C. and Blatt, M. R. (2012). A 2in1 cloning system enables ratiometric bimolecular fluorescence complementation (rBiFC). *BioTechniques* **53**, 311-314. doi:10.2144/000113941

Grossoehme, N. E., Akilesh, S., Guerinot, M. L. and Wilcox, D. E. (2006). Metal-binding thermodynamics of the histidine-rich sequence from the metal-transport protein IRT1 of *Arabidopsis thaliana*. *Inorg. Chem.* **45**, 8500-8508. doi:10.1021/ic0606431

Guerinot, M. L. (2000). The ZIP family of metal transporters. *Biochim. Biophys. Acta* **1465**, 190-198. doi:10.1016/S0005-2736(00)00138-3

Heucken, N. and Ivanov, R. (2018). The retromer, sorting nexins and the plant endomembrane protein trafficking. *J. Cell Sci.* **131**, jcs203695. doi:10.1242/jcs.203695

Hornbergs, J., Montag, K., Loschwitz, J., Mohr, I., Poschmann, G., Schnake, A., Gratz, R., Brumbarova, T., Eutebach, M., Angrand, K., C. et al. (2023). SEC14-GOLD protein PATELLIN2 binds IRON-REGULATED TRANSPORTER1 linking root iron uptake to vitamin E. *Plant Physiol.* **192**: 504-526. doi:10.1093/plphys/kiac563

Hu, J. (2021). Toward unzipping the ZIP metal transporters: structure, evolution, and implications on drug discovery against cancer. *FEBS J.* **288**, 5805-5825. doi:10.1111/febs.15658

Ismail, S. A., Vetter, I. R., Sot, B. and Wittinghofer, A. (2010). The Structure of an Arf-ArfGAP Complex Reveals a Ca^{2+} Regulatory Mechanism. *Cell* **141**, 812-821. doi:10.1016/j.cell.2010.03.051

Ismail, S. A., Chen, Y. X., Rusinova, A., Chandra, A., Bierbaum, M., Gremer, L., Triola, G., Waldmann, H., Bastiaens, P. I. and Wittinghofer, A. (2011). Arl2-GTP and Arl3-GTP regulate a GDI-like transport system for farnesylated cargo. *Nat. Chem. Biol.* **7**, 942-949. doi:10.1038/nchembio.686

Ivanov, R. and Vert, G. (2021). Endocytosis in plants: Peculiarities and roles in the regulated trafficking of plant metal transporters. *Biol. Cell* **113**, 1-13. doi:10.1111/boc.202000118

Ivanov, R., Brumbarova, T., Blum, A., Jantke, A.-M., Fink-Straube, C. and Bauer, P. (2014). SORTING NEXIN1 is required for modulating the trafficking and stability of the Arabidopsis IRON-REGULATED TRANSPORTER1. *Plant Cell* **26**, 1294-1307. doi:10.1105/tpc.113.116244

Jaillais, Y., Fobis-Loisy, I., Miège, C., Rollin, C. and Gaude, T. (2006). AtSNX1 defines an endosome for auxin-carrier trafficking in Arabidopsis. *Nature* **443**, 106-109. doi:10.1038/nature05046

Kerkeb, L., Mukherjee, I., Chatterjee, I., Lahner, B., Salt, D. E. and Connolly, E. L. (2008). Iron-induced turnover of the Arabidopsis IRON-REGULATED TRANSPORTER1 metal transporter requires lysine residues. *Plant Physiol.* **146**, 1964-1973. doi:10.1104/pp.107.113282

Khan, I., Gratz, R., Denezhkin, P., Schott-Verdugo, S. N., Angrand, K., Genders, L., Basgaran, R. M., Fink-Straube, C., Brumbarova, T., Gohlke, H.P. et al. (2019). Calcium-promoted interaction between the C2-domain protein EHB1 and metal transporter IRT1 inhibits Arabidopsis iron acquisition. *Plant Physiol.* **180**: 1564-1581. doi:10.1104/pp.19.00163

Kleine-Vehn, J., Dhonukshe, P., Sauer, M., Brewer, P. B., Wiśniewska, J., Paciorek, T., Benková, E. and Friml, J. (2008). ARF GEF-dependent transcytosis and polar delivery of PIN auxin carriers in Arabidopsis. *Curr. Biol.* **18**, 526-531. doi:10.1016/j.cub.2008.03.021

Knauer, T., Dümmer, M., Landgraf, F. and Forreiter, C. (2011). A negative effector of blue light-induced and gravitropic bending in Arabidopsis. *Plant Physiol.* **156**, 439-447. doi:10.1104/pp.110.167411

Kolb, C., Nagel, M.-K., Kalinowska, K., Hagmann, J., Ichikawa, M., Anzenberger, F., Alkofer, A., Sato, M. H., Braun, P. and Isono, E. (2015). FYVE1 is essential for vacuole biogenesis and intracellular trafficking in Arabidopsis. *Plant Physiol.* **167**, 1361-1373. doi:10.1104/pp.114.253377

Le, C. T. T., Brumbarova, T., Ivanov, R., Stoof, C., Weber, E., Mohrbacher, J., Fink-Straube, C. and Bauer, P. (2015). Zinc finger of Arabidopsis thaliana12 (ZAT12) Interacts with fer-like iron deficiency-induced transcription factor (FIT) linking iron deficiency and oxidative stress responses. *Plant Physiol.* **170**, 540-557.

Li, W., Feng, Y., Hao, C., Guo, X., Cui, Y., He, M. and He, X. (2007). The BLOC interactomes form a network in endosomal transport. *J. Genet. Genomics* **34**, 669-682. doi:10.1016/S1673-8527(07)60076-9

Martín-Barranco, A., Spielmann, J., Dubeaux, G., Vert, G. and Zelazny, E. (2020). Dynamic control of the high-affinity iron uptake complex in root epidermal cells. *Plant Physiol.* **184**, 1236-1250. doi:10.1104/pp.20.00234

Mayer, U., Herzog, U., Berger, F., Inzé, D. and Jürgens, G. (1999). Mutations in the PILZ group genes disrupt the microtubule cytoskeleton and uncouple cell cycle progression from cell division in Arabidopsis embryo and endosperm. *Eur. J. Cell Biol.* **78**, 100-108. doi:10.1016/S0171-9335(99)80011-9

McElver, J., Patton, D., Rumbaugh, M., Liu, C.-m., Yang, L. J. and Meinke, D. (2000). The TITAN5 gene of Arabidopsis encodes a protein related to the ADP ribosylation factor family of GTP binding proteins. *Plant Cell* **12**, 1379-1392. doi:10.1105/tpc.12.8.1379

Memon, A. R. (2004). The role of ADP-ribosylation factor and SAR1 in vesicular trafficking in plants. *Biochim. Biophys. Acta* **1664**, 9-30. doi:10.1016/j.bbamem.2004.04.005

Mohr, I., Mirzaiebadizi, A., Sanyal, S. K., Chuenban, P., Ahmadian, M. R., Ivanov, R. and Bauer, P. (2024). Characterization of the small Arabidopsis thaliana GTPase and ADP-ribosylation factor-like 2 protein TITAN 5. *J. Cell Sci.* **137**, jcs262315. doi:10.1242/jcs.262315

Montag, K., Hornbergs, J., Ivanov, R. and Bauer, P. (2020). Phylogenetic analysis of plant multi-domain SEC14-like phosphatidylinositol transfer proteins and structure–function properties of PATELLIN2. *Plant Mol. Biol.* **104**, 665-678. doi:10.1007/s11103-020-01067-y

Montag, K., Ivanov, R. and Bauer, P. (2023). Role of SEC14-like phosphatidylinositol transfer proteins in membrane identity and dynamics. *Front. Plant Sci.* **14**, 1181031. doi:10.3389/fpls.2023.1181031

Mori, R. and Toda, T. (2013). The dual role of fission yeast Tbc1/cofactor C orchestrates microtubule homeostasis in tubulin folding and acts as a GAP for GTPase Alp41/Arl2. *Mol. Biol. Cell* **24**: 1713-1724, s1711-1718. doi:10.1091/mbc.e12-11-0792

Nielsen, E. (2020). The Small GTPase Superfamily in Plants: A Conserved Regulatory Module with Novel Functions. *Annu. Rev. Plant Biol.* **71**, 247-272. doi:10.1146/annurev-arplant-112619-025827

Ohwaki, Y. and Sugahara, K. (1997). Active extrusion of protons and exudation of carboxylic acids in response to iron deficiency by roots of chickpea (Cicer arietinum L. *Plant Soil* **189**, 49-55. doi:10.1023/A:1004271108351

Peter, B. J., Kent, H. M., Mills, I. G., Vallis, Y., Butler, P. J., Evans, P. R. and McMahon, H. T. (2004). BAR domains as sensors of membrane curvature: the amphiphysin BAR structure. *Science* **303**, 495-499. doi:10.1126/science.1092586

Pourcher, M., Santambrogio, M., Thazar, N., Thierry, A.-M., Fobis-Loisy, I., Miège, C., Jaillais, Y. and Gaude, T. (2010). Analyses of sorting nexins reveal distinct retromer-subcomplex functions in development and protein sorting in *Arabidopsis thaliana*. *Plant Cell* **22**, 3980-3991. doi:10.1105/tpc.110.078451

Radcliffe, P. A., Vardy, L. and Toda, T. (2000). A conserved small GTP-binding protein Alp41 is essential for the cofactor-dependent biogenesis of microtubules in fission yeast. *FEBS Lett.* **468**, 84-88. doi:10.1016/S0014-5793(00)01202-3

Raposo, G., Marks, M. S. and Cutler, D. F. (2007). Lysosome-related organelles: driving post-Golgi compartments into specialisation. *Curr. Opin. Cell Biol.* **19**, 394-401. doi:10.1016/j.ceb.2007.05.001

Rath, M., Dümmer, M., Galland, P. and Forreiter, C. (2020). A gravitropic stimulus alters the distribution of EHB1, a negative effector of root gravitropism in Arabidopsis. *Plant Direct* **4**, e00215. doi:10.1002/pld3.215

Robinson, N. J., Procter, C. M., Connolly, E. L. and Guerinot, M. L. (1999). A ferric-chelate reductase for iron uptake from soils. *Nature* **397**, 694-697. doi:10.1038/17800

Rodriguez, L., Gonzalez-Guzman, M., Diaz, M., Rodrigues, A., Izquierdo-Garcia, A. C., Peirats-Llobet, M., Fernandez, M. A., Antoni, R., Fernandez, D., Marquez, J. A. et al. (2014). C2-domain abscisic acid-related proteins mediate the interaction of PYR/PYL/RCAR abscisic acid receptors with the plasma membrane and regulate abscisic acid sensitivity in Arabidopsis. *Plant Cell* **26**, 4802-4820. doi:10.1105/tpc.114.129973

Schmid, N. B., Giehl, R. F., Döll, S., Mock, H. P., Strehmel, N., Scheel, D., Kong, X., Hider, R. C. and von Wirén, N. (2014). Feruloyl-CoA 6'-Hydroxylase1-dependent coumarins mediate iron acquisition from alkaline substrates in Arabidopsis. *Plant Physiol.* **164**, 160-172. doi:10.1104/pp.113.228544

Schneider, C. A., Rasband, W. S. and Eliceiri, K. W. (2012). NIH Image to ImageJ: 25 years of image analysis. *Nat. Methods* **9**, 671-675. doi:10.1038/nmeth.2089

Sharer, J. D., Shern, J. F., Van Valkenburgh, H., Wallace, D. C. and Kahn, R. A. (2002). ARL2 and BART Enter mitochondria and bind the adenine nucleotide transporter. *Mol. Biol. Cell* **13**, 71-83. doi:10.1091/mbc.01-05-0245

Shin, L.-J., Lo, J.-C., Chen, G.-H., Callis, J., Fu, H. and Yeh, K.-C. (2013). IRT1 Degradation factor1, a RING E3 ubiquitin ligase, regulates the degradation of iron-regulated transporter1 in Arabidopsis. *Plant Cell* **25**, 3039-3051. doi:10.1105/tpc.113.115212

Steinmann, T., Geldner, N., Grebe, M., Mangold, S., Jackson, C. L., Paris, S., Gälweiler, L., Palme, K. and Jürgens, G. (1999). Coordinated polar localization of auxin efflux carrier PIN1 by GNOM ARF GEF. *Science* **286**, 316-318. doi:10.1126/science.286.5438.316

Sztul, E., Chen, P.-W., Casanova, J. E., Cherfils, J., Dacks, J. B., Lambright, D. G., Lee, F.-J. S., Randazzo, P. A., Santy, L. C., Schürmann, A. et al. (2019). ARF GTPases and their GEFs and GAPs: concepts and challenges. *Mol. Biol. Cell* **30**, 1249-1271. doi:10.1091/mbc.E18-12-0820

Takano, J., Tanaka, M., Toyoda, A., Miwa, K., Kasai, K., Fuji, K., Onouchi, H., Naito, S. and Fujiwara, T. (2010). Polar localization and degradation of Arabidopsis boron transporters through distinct trafficking pathways. *Proc. Natl. Acad. Sci. USA* **107**, 5220-5225. doi:10.1073/pnas.0910744107

Tanaka, H., Kitakura, S., De Rycke, R., De Groodt, R. and Friml, J. (2009). Fluorescence imaging-based screen identifies ARF GEF component of early endosomal trafficking. *Curr. Biol.* **19**, 391-397. doi:10.1016/j.cub.2009.01.057

Tanaka, H., Nodzyński, T., Kitakura, S., Feraru, M. I., Sasabe, M., Ishikawa, T., Kleine-Vehn, J., Kakimoto, T. and Friml, J. (2014). BEX1/ARF1A1C is required for BFA-sensitive recycling of PIN auxin transporters and auxin-mediated development in Arabidopsis. *Plant Cell Physiol.* **55**, 737-749. doi:10.1093/pcp/pct196

Tzafrir, I., McElver, J. A., Liu Cm, C.-m., Yang, L. J., Wu, J. Q., Martinez, A., Patton, D. A. and Meinke, D. W. (2002). Diversity of TITAN functions in Arabidopsis seed development. *Plant Physiol.* **128**, 38-51. doi:10.1104/pp.010911

Valencia, J. P., Goodman, K. and Otegui, M. S. (2016). Endocytosis and endosomal trafficking in plants. *Annu. Rev. Plant Biol.* **67**, 309-335. doi:10.1146/annurev-arplant-043015-112242

Vernoud, V., Horton, A. C., Yang, Z. and Nielsen, E. (2003). Analysis of the small GTPase gene superfamily of Arabidopsis. *Plant Physiol.* **131**, 1191-1208. doi:10.1104/pp.013052

Vert, G., Grotz, N., Dédaldéchamp, F., Gaymard, F., Guerinot, M. L., Briat, J.-F. and Curie, C. (2002). IRT1, an Arabidopsis transporter essential for iron uptake from the soil and for plant growth. *Plant Cell* **14**, 1223-1233. doi:10.1105/tpc.001388

von der Mark, C., Ivanov, R., Eutebach, M., Maurino, V. G., Bauer, P. and Brumbarova, T. (2020). Reactive oxygen species coordinate the transcriptional responses to iron availability in Arabidopsis. *J. Exp. Bot.* **72**, 2181-2195. doi:10.1093/jxb/eraa522

Yoshinari, A., Toda, Y. and Takano, J. (2021). GNOM-dependent endocytosis maintains polar localisation of the borate exporter BOR1 in Arabidopsis. *Biol. Cell* **113**, 264-269. doi:10.1111/boc.202000106